BALOGUN, Y., IYI, D., FAISAL, N., OYENEYIN, B., OLUYEMI, G. and MAHON, R. 2021. Experimental investigation of the effect of temperature on two-phase oil-water relative permeability. *Journal of petroleum science and engineering* [online], 203, article ID 108645. Available from: https://doi.org/10.1016/j.petrol.2021.108645

Experimental investigation of the effect of temperature on two-phase oil-water relative permeability.

BALOGUN, Y., IYI, D., FAISAL, N., OYENEYIN, B., OLUYEMI, G. and MAHON, R.

2021

Experimental investigation of the effect of temperature on two-phase oil-water relative permeability

Yakubu Balogun[1*], Draco Iyi[2], Nadimul Faisal[1], Babs Oyeneyin[1], Gbenga Oluyemi[1], Ruissein Mahon[1]

[1*] School of Engineering, Robert Gordon University Aberdeen, AB10 7GJ, United Kingdom Email: y.balogun@rgu.ac.uk
[2]School of Energy, Construction & Environment
Coventry University, CV1 5FB, United Kingdom

Abstract-

Relative permeability is affected by several flow parameters, mainly the operating temperature and fluid viscosity. Fluid viscosities change with temperature, which correspondingly affects the relative permeability. Temperature is believed to have a considerable effect on oil–water relative permeability, thus a vital input parameter in petroleum reservoir production modelling. The actual effect of temperature on oil-water relative permeability curves has been a subject of debate within the scientific community. The literature shows contradictory experimental and numerical results concerning the effect of temperature on oil-water relative permeability. This work investigates the effect of temperature on oil-water relative permeability using well-sorted unconsolidated silica sandpacks, by adopting the unsteady-state relative permeability method, and by applying numerical history matching technique. The series of experiments were conducted at different temperatures of 40, 60, and 80 °C under three levels of injection flow rate (0.0083, 0.0125, 0.0167 cm^3/s) for two different oil samples. The findings show that oil-water relative permeability is a function of temperature, water injection flow rate and oil viscosity. Generally, the profile of oil and water relative permeability curve changes with varying temperature, oil viscosity and water injection flow rate at the same operating condition.

Key words: Multiphase flow, Relative permeability, Temperature, Porous media flow, Empirical model, History matching

Nomenclature

A	Area (cm^2)
K	Permeability (m^2 or D)
L	Length (cm)
NPV	Number of pore volume
P	Pressures (atm)
q	Flow rate (cm^3/s)
Sor	Irreducible oil saturation
M	Mobility ratio
S	Saturation
t	Time (s)
T	Temperature (K)
v	Volume (cm^3)

Greek symbols

∅	Porosity (dimensionless)
λ	Fluid mobility
σ	Interfacial tension (dyne/cm)
∝	Volume fraction (dimensionless)
μ	Viscosity(cp)
ρ	Density (kg/m^3)

Subscript

b	Bulk
o	Oil
or	Residual oil
p	Pore
c	Capillary
r	Relative
w	Water
w_i	Initial water

Graphical Abstract

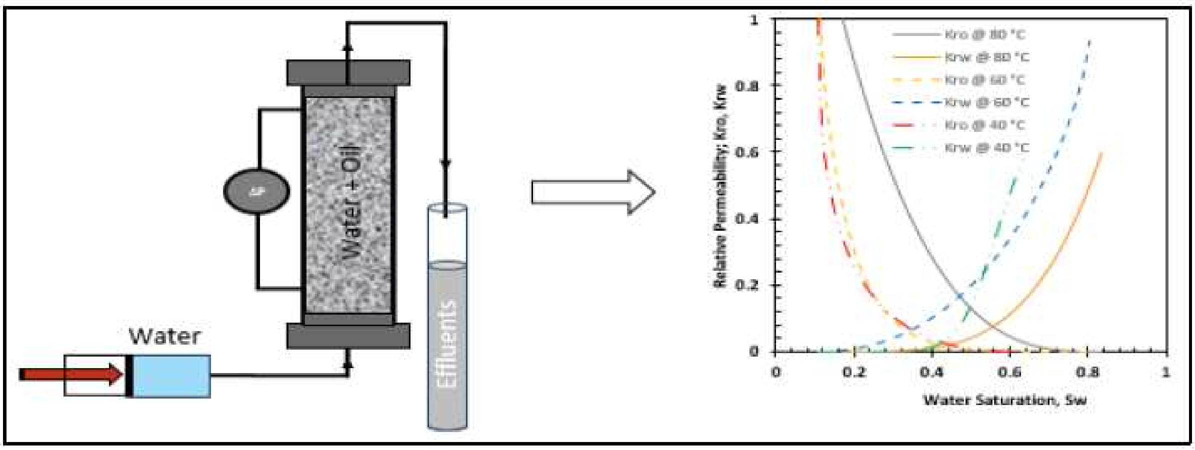

1.0 Introduction

Multiphase flow of fluid through porous media is a complex phenomenon that is often poorly understood. Relative permeability is a dimensionless multiphase flow parameter that explains the relative propensity of a fluid to flow in the presence of another. It is one of the most important factors influencing fluid behaviour through a porous medium and provides an indication of the complicated pore-level displacement physics coupled with the fluid-fluid and solid-fluid interaction. Relative permeability is affected by several factors: viscosity, interfacial tension, fluid saturation, wettability, and rock properties. These properties are themselves affected by temperature (Esmaeili et al., 2019a). Therefore, it is logical to assume that temperature will have some significant effect on relative permeability.

Currently, the same values of oil-water relative permeability are used in reservoir simulators at different temperatures. This would potentially lead to significant errors and unrealistic values in the predictions. At elevated temperatures, some rock grains may expand while some particles are detached and re-mobilized in unconsolidated media which results in opening of more pore spaces or blockage of the pore throat and increment in the pore constriction thereby reducing the intrinsic permeability of the rock. Thermal stress induced when there is a sharp temperature contrast in a system is believed to affect the properties of the media and needs to be properly understood to aid engineering applications.

Although relative permeability is believed to vary with temperature, there is controversy on the effect and thus the same set of relative permeability is often applied in the prediction of reservoir performance at varying temperature (Qin et al., 2018). Several factors have varying effect on the relative permeability curve. Microscopic factors ranging from media wettability, fluid-fluid interfacial tension, and pore size distribution of the porous media. All these factors can potentially change the shape of relative permeability curves. While some authors believe that relative permeability does not change with temperature (Sufi et al., 1982; Miller and Ramey, 1985; Polikar et al., 1990; Akin et al., 1998); arguing that the observed variation in values is a function of other fluid-fluid or fluid-rock interactions and not necessarily the temperature factor, others disagree maintaining that the same relative permeability cannot be used for different temperature conditions (Torabzadey, 1984; Watson and Ertekin, 1988; Maini et al., 1989; Sola et al., 2007).

Several techniques ranging from laboratory experiments, mathematical models and empirical correlations have been adopted for relative permeability measurements. Laboratory measurement of relative permeability typically involves the use of a small porous sample and generating one-dimensional two-phase flow in the sample from an inlet to an outlet. There are three different experimental measurement methods for relative permeability namely, steady-state, unsteady-state and centrifuge.

The steady-state approach involves the concurrent injection of all fluid phases (water and oil or water, oil and gas) into a porous medium at different metered fractional flows. With each run for the pre-set fractional flows, the flow domain is allowed to reach steady-state, (indicated by constant stable pressure drop across the sample). The unsteady-state method on the other hand involves the injection of a single fluid into the porous media during each displacement process while monitoring the recovery of phases at the outlet with the corresponding pressure drop across the sample. Some of the challenges in the steady-state method are that the steady-state procedure is not an exact representation of the recovery process in an underground reservoir as well as it being time-consuming and costly (Polikar et al., 1990; Sola et al., 2007; Zeidani and Maini, 2016).

Unlike the steady-state method, the unsteady-state is an indirect technique for computing the relative permeability. It involves the application of the Buckley-Leverett theory (Buckley and Leverett, 1942) for linear displacement of immiscible and incompressible fluids (Honarpour and Mahmood, 1988). Due to the considerably less time involved, the unsteady-state method is widely used for relative permeability measurements, however, this method is prone to experimental and interpretation errors (Ali, 1997). Interpretation of the unsteady-state experimental data for relative permeability calculations involves various mathematical (Johnson et al., 1959), graphical (Jones and Roszelle, 1978) and numerical history matching techniques (Archer and Wong, 1973; Lenormand et al., 2016).

Maini and Okazawa (1987) performed a series of unsteady-state two-phase experiments on unconsolidated silica sand using Bodo stock tank oil with relative permeability computed using the history matching technique. The conclusion from the study is similar to earlier reports with relative permeability increasing with temperature. Three-phase flow experiments were performed for measuring relative permeability at elevated temperatures and pressures by Maini et al., (1989) using Ottawa sand as the porous media with refined mineral oil, distilled water and nitrogen gas as the fluid phases. A steady-state approach was adopted for the different experiments at an elevated temperature of 100 ^{o}C and pressure of 3.5 MPa. Unlike the earlier two-phase experiments, no dependence on temperature was reported in this study with the findings showing that the three-phase water and gas relative permeability are functions of their respective saturations only and did not change with the direction of saturation change. The oil relative permeability on the other hand was reported to vary as the saturation of the other fluids changed.

Kumar and Inouye (1994) carried out unsteady-state experiments aimed at developing and evaluating simpler low-temperature analogues of the high temperature relative permeability data using similar viscosity ratio and wettability. The JBN method was used for computing the relative permeability and results show that the endpoint saturation changes with viscosity ratio but remains unchanged under varying temperature.

Sufi et al. (1982) presented an experimental study on the temperature effects on oil-water relative permeability and reported that the relative permeability curves remain unchanged with temperature. The same observation was reported by Miller and Ramey (1985) after conducting dynamic-displacement laboratory experiments on unconsolidated and consolidated porous media with water and a refined white mineral oil to measure relative permeability to oil and water. The experiments were carried out on cores of 5.1 cm in diameter and 52 cm in length with temperatures ranging from room temperature to about 149 °C. Results presented show essentially no changes in the relative permeability curves with temperature variations. They argued that factors such as viscous instabilities, capillary end effects or possible challenge in maintaining material balances might have affected previous reported results.

Akin et al. (1998) alluded to the argument of Miller and Ramey (1985) by stating that there is the need for examining the suitability of applying the JBN method for heavy oil/water relative permeability calculations while investigating the effect of temperature on relative permeability through numerical and experimental methods. They stated that the use of the JBN technique results in an erroneous result showing some temperature dependence of relative permeability curves. Unsteady-state relative permeability experiments were performed for heavy oil and brine at different temperatures of 22 and 66 ^{o}C. They showed that a single set of relative permeability curves is representative of both the ambient and high temperature for the experiments performed and thus concluded that relative permeability is not a function of temperature. Polikar et al. (1990) also supports this claim as they found no significant temperature effects from their experiments on Athabasca bitumen-water system.

Zhang et al. (2017) conducted a series of core flooding experiments on five sandstone core samples having different permeability values at different temperatures, to investigate the relationship between relative permeability curves and temperature. As laboratory state conditions cannot perfectly represent fluid flow behaviour under reservoir condition, they proposed a way of translating the laboratory results to reservoir scales by combing the JBN method with an empirical method. The study observed a significant increment in the shape of oil and water relative permeability curves with a rise in temperature for the various core samples with different permeability. With an increase in temperature, residual oil saturation was observed to decrease nonlinearly while the irreducible water saturation increased linearly but decreased with reducing permeability.

Akhlaghinia et al. (2014) conducted core flood experiments on consolidated sandstone core samples to measure relative permeability using heavy oil, methane and carbon dioxide and used the JBN technique to calculate two-phase relative permeability. A series of experiments were conducted at three different temperatures values of 28, 40, and 52 °C for different fluid pairs to investigate temperature effect on relative permeability curves. Experimental results showed a linear increase of about 65% and 50% in the water relative permeability for temperatures ranging from 28 to 40 °C and 40 to 52 °C, respectively. While the oil relative permeability curve increased at a rate of about 70% with a temperature change from 28 to 40 °C and decreased by about 30% with a temperature increase from 40 to 52 °C.

Kovscek and Vega (2014) carried out a series of steady-state core flood on low-permeability consolidated core samples to investigate the dependency of the respective phase relative permeability on operating temperature ranging from 45 to 230 ^{o}C. The study reported a systematic shift to increased water-wet state with increasing temperature. It was observed that this water wetness affects the relative permeability with the water-phase relative permeability shifting to the right as the temperature increases. Similar temperature range was investigated by Zeidani and Maini (2016) with Athabasca reservoir oil using the displacement experimental approach and history matching of the data. The reported results showed a decrease in oil saturation with increase in temperature.

Ashrafi et al. (2014) investigated the dependency of oil and water relative permeability for heavy oil systems with temperature using unconsolidated media made up of glass beads and sandpacks. The study reported that both the oil and water relative permeability is not affected by temperature. While changes to the fluid relative permeability were observed, the study suggests that the relative permeability variations with temperature is mainly due to the oil to water viscosity ratio changes with temperature. The study therefore concluded that temperature dependency of relative permeability is due more to different conditions such as viscous instabilities or fingering in higher permeable cores as well as viscosity ratios than fundamental flow properties.

Qin et al. (2018) reported experimental results on the effects of temperature on oil and water relative permeability in heavy-oil reservoirs in unconsolidated porous systems stating that irreducible water saturation linearly increases as temperature increases while the residual oil saturation decreases non-linearly. In agreement with previous reports, this study showed that the water-wettability of the porous systems is increased, and overall relative permeability curves shift to the right with increasing temperature with both oil and water relative permeability increasing but the increase ratio of water less than that of oil. A summary table of the experimental studies, methods, operating conditions, and temperature dependency on relative is been presented in Table 1.

Table 1: Summary of literature reports on the effect of temperature on relative permeability.

	Reference	Materials		Method	Operating conditions		Effect of temperature on relative permeability
		Porous media	Fluid		Temperature (^oC)	Pressure (psi)	
1	Sufi et al. (1982)	Unconsolidated sandstone	Refined oil	USS (JBN and Welge)	Up to 149	2000	No effect
2	Torabzadeh and Handy (1984)	Berea sandstone	Dodecanese	USS and SS	$21 \leq T \leq 177$	650	K_{ro} increases and K_{rw} decreases
3	Miller and Ramey (1985)	Ottawa and Berea sands	Refined oil	-	$19 \leq T \leq 149$	500	No effect
4	Maini and Batycky (1985)	Sandstone	Heavy oil	USS, History matching	$25 \leq T \leq 272$	1100	Reduction in K_{ro} and K_{rw} remain unchanged
5	Kumar et al. (1985)	Berea sandstone Peace River sand	Dodecanese	Theoretical	Up to 177	-	K_{ro} increases and K_{rw} decreases K_r curve affected
6	Closmann et al. (1988)	Berea sandstone	Unaltered, thermally altered and deasphalted tar	SS	$62 \leq T \leq 169$	-	-
7	Watson and Ertekin (1988)	Ottawa silica	Refined oil	SS	$104 \leq T \leq 149$	-	Reduction of K_{ro} and K_{rw} due to formation of third Phase
8	Maini et al. (1989)	Berea sand	Refined oil	USS (history matching)	100	-	K_r curve affected
9	Polikar et al. (1990)	Athabasca sandstone	Heavy oil	SS and USS	$100 \leq T \leq 250$	-	No effect
10	Kumar and Inuouye (1994)	Unconsolidated sandstone	White, refined and heavy oil	USS (JBN)	$24 \leq T \leq 160$	-	-
11	Akin et al. (1998)	Ottawa sandstone and sandpack	Mineral oil	Simulation	$22 \leq T \leq 66$	-	No effect
12	Esfahani and Haghighib	Dolomite and limestone	Light oil	USS (JBN)	$16 \leq T \leq 104$	-	Increasing temperature makes rocks oil-wet

	(2004)						
13	Schembre et al. (2005)	Diatomite cores	Mineral and crude oil	USS	$120 \leq T \leq 180$	-	Media becomes more water wet with K_{rw} and K_{ro} affected by temperature
14	Sola et al. (2007)	Dolomite	Heavy oil	USS	$38 \leq T \leq 260$	2500	K_{ro} becomes more linear and K_{rw} reduces
15	Hamouda et al. (2008)	Chalk core sample	n-decane	Jones and Rosezelle	Up to 130	-	Kr shifts to right at about 80 ^oC as more water wet but shifts to oil wet state at about 130 ^oC
16	Hamouda and Karoussi (2008)	Chalk core samples	-	Simulation	$23 \leq T \leq 130$	-	Effects due to experimental artefacts
17	Ashrafi et al. (2014)	Unconsolidated sandpacks	Athabasca bitumen	USS History matching	Up to 300	363	K_r affected by temperature
18	Kovscek and Vega (2014)	Siliceous shale	Dehydrated dead oil	SS	$45 \leq T \leq 230$	-	K_{rw} shifts to the right as temperature increases
19	Akhlaghinia et al. (2014)	Consolidated sandstone core	Heavy oil	JBN method	$28 \leq T \leq 52$	-	K_{rw} and K_{ro} increases as temperature rises to about 40 ^oC, K_{ro} decreases when temperature reaches 52 ^oC
20	Zeidani and Maini (2016)	Unconsolidated sandpack	Athabasca reservoir oil	USS History matching	Up to 220	-	Residual oil saturation decreases with temperature
21	Cao et al. (2016)	Consolidated reservoir cores	Waxy crude oil	USS	$50 \leq T \leq 85$		K_{rw} and K_{ro} increases with temperature
22	Qin et al. (2018)	Unconsolidated sandpacks	Heavy oil	USS	$45 \leq T \leq 200$		-

Based on the review conducted, it is apparent that there exist a series of complex interrelationships between the fluids and the porous material properties through which they flow, and ample research focus has been given to explain these occurrences. Attempts have been made to establish the fundamental understanding of these phenomena through controlled laboratory experiments and empirical modelling by applying established correlations in literature. Numerous researchers have studied the effect of temperature and other parameters on two-phase relative permeability in porous media and reported contradictory results; while some reported a dependence of one or two parameters, others showed independency. The aim of this study is to investigate the effect of varying temperature on oil-water relative permeability and to developed empirical constants for an established correlation to be used under a specific range of conditions.

2.0 Experimental methodology

This section gives a detailed description on the experimental materials, apparatus setup and procedure followed in this study.

2.1. Material

2.1.1 Rock properties

The porous media used for all the test in the study is made up of unconsolidated commercial grade silica sand (20/40 mesh size). An unconsolidated system has been used mainly due to the relative ease of flooding viscous oil without building up high pressures at the injection face. Table 2 shows the physical properties of a typical commercial grade 20/40 silica sand.

Table 2: Physical properties of silica sand used for this study.

Typical physical properties of the sand sample	
Colour	White
Grain shape	Round
Hardness (Mohs)	7
Melting point (°C)	1710
Mineral	Quartz
Bulk density	1.68 g/cc
Specific gravity	2.65 g/cc
pH	7

The packing of the sand column was carried out in such a way as to produce a homogeneous column as well as restoring the bulk density of the column to a value similar to that naturally observed, while also minimising the formation of preferential flow pathways. The core-holder was placed vertically upwards on a mechanical vibrator to aid in settling of the pack while the sand was being poured. From the top of the holder, the sand was poured with a funnel as the vibrator allowed it to distribute and settle uniformly in the core-holder (Figure 1). To prevent influx of fines from the core-holder to the flow lines, 0.25-micron mesh were fixed at both ends before connecting the ends caps. The weight method was used for the porosity measurement of the sandpack. The bulk volume (V_b) of the media is determined as the internal volume of the core-holder was computed as the volume of a cylinder from its dimensions. The volume of the sand mass was determined by using the relationship between density, mass and volume while taking the density of 2.65 g/cm^3 for silica sand as seen in literature (Satter et al., 2008). The pore volume of the porous cell was then computed by subtracting the grain volume determined earlier from the bulk volume. The porosity of the porous medium was subsequently calculated using the pore volume and bulk volume with the Eq. 1.

$$Porosity\ (\emptyset) = \frac{Pore\ volume\ (V_p)}{Bulk\ volume\ (V_b)} = \frac{Bulk\ volume - Grain\ volume}{Bulk\ Volume} \qquad 1$$

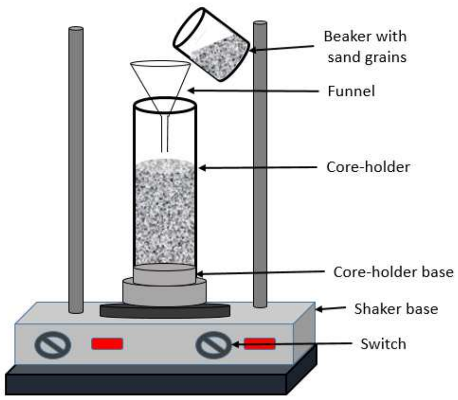

Figure 1: Schematic of the core-holder on the mechanical vibrator showing the sand packing process.

After determining the samples' pore volume and porosity, the absolute permeability to brine was experimentally determined under a single-phase flow scenario. In computing absolute permeability, brine was injected into the porous system at a specified flow rate and the pressure differentials (measured with the aid of installed pressure transducers) were noted and recorded when the flow had attained a steady-state conditions, that is, a constant flow rate was attained at the inlet and outlet. Brine has been used since a fundamental assumption for the absolute permeability test in porous media is that the permeability of a porous media is an integral property of the medium and is not dependent on the fluid used in its measurement provided that the flow rate is proportional to the pressure gradient (Klinkenberg, 1941). Miller and Ramey (1985) reported in their study that the effect of temperature on the absolute permeability of an unconsolidated core is negligible at temperatures below 200 ^{o}C. The study reported approximately 2% increase at 200°F (93°C) above permeability measured at room temperature, consequently, temperature effects on the porous media's absolute permeability has not considered. A similar result was reported by Talreja et al. (2020), stating that temperature causes changes in physical and mechanical properties of rocks resulting in instability at temperatures above 200 °C.

Core absolute permeability to brine from the pressure and flow rate data was calculated using Darcy's law (Eq. 2):

$$k = \frac{q\mu}{A} \cdot \frac{L}{\Delta P} \qquad 2$$

Where k is the absolute permeability to brine in Darcy; μ is the fluid viscosity in cp; ΔP is the pressure drop in atm across a porous length L in cm under a volumetric flow rate, q in cm^3/s; and A the cross-sectional area of the injection face in cm^2.

2.1.2 Fluid properties

The test fluid used for the experiments are mainly brine and oil. While the brine is divided into two categories; synthetic formation water and synthetic seawater; the oil sample is in two categories namely and Shell Rimula R4 L 15W - 40 engine oil, and mineral oil. These fluids are chosen because of the high level of immiscibility, ease of handling, and well-known or easily determined properties.

Brine samples

In this study, two different synthetic brine samples are prepared to simulate the formation water (FW) inside the porous sample before flooding and seawater (SW) to simulate the seawater used for water injection during the core flooding process. The brine solutions are prepared in the lab using deionized water and appropriate amounts of sodium chloride (NaCl), anhydrous calcium chloride ($CaCl_2$), potassium chloride (KCl), sodium hydrogen carbonate ($NaHCO_3$) and magnesium chloride hexahydrate ($MgCl_2.6H_2O$) analytical grade salts. The concentration of each salt in the synthesised brine is adapted from Oluyemi (2014) and Rostami et al. (2019) and shown in Table 3 and Table 4 with the dissolved salt concentration expressed in parts per million on a mass basis (ppm). Preceding the usage of the synthetic brine, the solution was filtered with 0.22 μm filter paper. This was done to ensure that no extraneous fines were introduced into the system which could interfere with the pump piston seals and check valves; and prevent undue pore blockage in the respective sandpacks.

Table 3: Physical properties of the fluid samples used for the experiments at ambient condition.

Fluid	Density (kg/m3)	Viscosity (cP)
Brine (SW)	1000	1.003
Brine (FW)	1020	1.005
Oil	850	147

Table 4: Chemical composition of the synthetic brine samples.

Salt (ppm)/Brine	Formation Water (FW)	Salt (ppm)/Brine	Seawater (SW)
NaCl	140316	NaCl	26400
$CaCo_3$	1628	$CaCl_2$	1180
$MgCl_2$	2856	KCl	400

$CaCl_2$	40287	$NaHCo_3$	7340
Na_2SO_4	2588	$MgCl_2.6H_2O$	5270
$NaHCO_3$	2016		

Oil samples

The viscosity of the oil sample was measured using a Fann 35 viscometer which is a typical Couette rotational viscometer capable of measuring the rheological properties of fluids: both Newtonian and non-Newtonian. The viscometer measures the viscosity as a function of shear rate. Fluid viscosities were measured at varying temperature ranges from 20 ^{O}C to 80 ºC. The Fann model 35 viscometer used is a direct-reading instrument in twelve speed designs. In this viscometer, the oil sample is contained in the annular space between an outer rotating cylinder and the bob (inner cylinder). For density measurements, the Anton-Paar portable density meter: DMA 35 was used. The device is capable of measuring fluid density at varying temperatures with density accuracy level 0.001 g/cm^3 and temperature of 0.2 ^{o}C. Figure 2 below shows the physical properties (density and viscosity) of the two oil samples at varying temperatures.

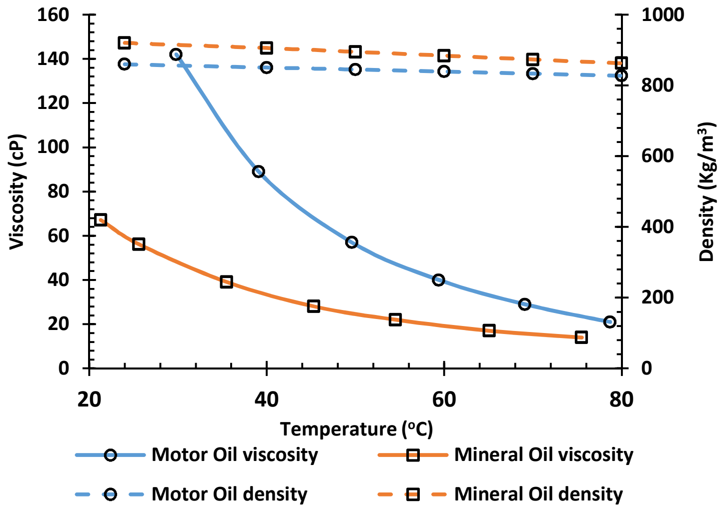

Figure 2: Plot of viscosity and density of oil sample against temperature at a shear rate of 510 s^{-1}.

2.2. Experimental setup

Figure 3 shows a schematic representation of the experimental setup used in this study. This setup was made up mainly of three sections: injection, core holder and production. Fluid was injected using a multi-solvent High-Performance Liquid Chromatography (HPLC) dual piston pump supplied by 220V. The pump is made of 316 stainless steel fitted with two 50 cm^3 pump heads with the capability of running at a wide range of flow rate from 0.00167 to 1.67 cm^3 with a 0.001 cm^3 increments and pressure range of 0- 68.046 atm with consistent performance at a flow accuracy of $\pm$2%. The two pump heads were connected to separate fluid bottles; one serving as the reservoir for the injection fluid (e.g. oil and brine), while the other was the flushing fluid made of 20 % methanol solution.

The core-holder used for this study was designed and fabricated in-house with a length of 10 cm, diameter of 5.1 cm and thickness of 1.9 cm (Figure 4). The core-holder's body was constructed of aluminum metal, the choice of material is mainly due to the lightweight of aluminum at 2.7 g/cm^3, and its thermal conductivity of 205 W/m-K coupled with the corrosion resistant nature of the metal.

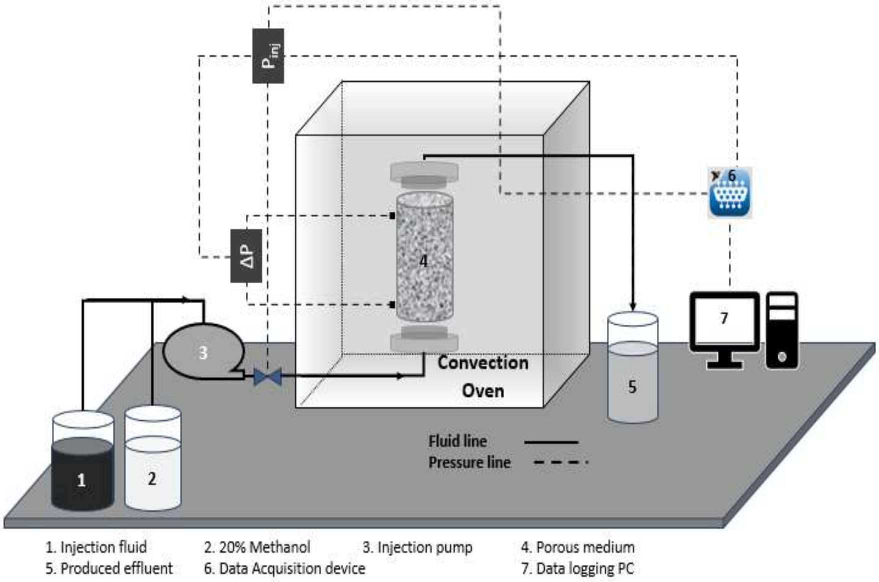

Figure 3: Schematic flow diagram of the experimental apparatus.

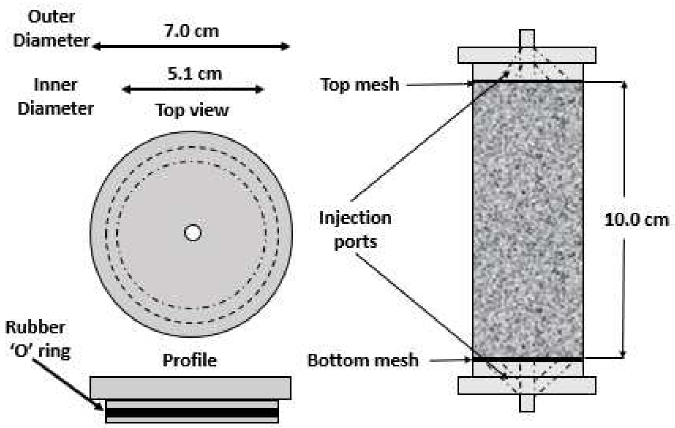

Figure 4: Diagrammatic representation of the aluminium core holder with its dimensions.

Pressure monitoring was achieved using a Micro-Machined Silicon Wet/Wet Differential Pressure Transducers supplied by Omega with measurements recorded electronically through the aid of a high-speed National Instruments Data Acquisition System (NIDAQ) NI 9212. The differential pressure transducer is of the range of 0-1.02 atm with an excitation voltage of 10 Vdc supplied by a

Weir 413D power supply. The transducer can operate within a temperature range of between -45 to 121°C. After setting up the pressure measuring system, the transducers were calibrated using a Druck device to ascertain the relationship between the electric voltage and pressure readings.

2.3. Experimental procedure

The core-holder packed with sand was placed inside the convection oven vertically and saturated with the synthetic formation brine using the HPLC pump. The absolute permeability of the packed sand to brine was measured at steady-state for each case at the specified test temperature using Eq. 2. The core was flooded with formation brine at different flow rates of 0.0083, 0.0125, and 0.0167 cm^3/s for approximately 45 mins each for the absolute permeability measurement, monitoring the linearity of the differential pressure variations with flow rate. After the imbibition process at 100% brine saturation, the drainage process was commenced with oil injected at 0.0167 cm^3/s to initialise the core and compute the initial water saturation (S_{wi}). Oil injection was continued after draining all the displaceable water and the differential pressure readings taken to compute the effective oil permeability. In the next step, the initialised core was imbibed with synthetic sea water at a specific flow rate. The rates used in this study are all approximately or less than 1 PV/hr as recommended by Polikar et al. (1990). During the water flood process, the cumulative produced oil and water was recorded at known time intervals and the differential pressure across the sandpack was equally monitored and recorded. The water injection was continued until oil production essentially ceased and the differential pressure across the core became stable. At the end of each run, several pore volumes of ethanol were injected to cleanse the flow lines. The sequence of flow is summarised in Figure 5 below.

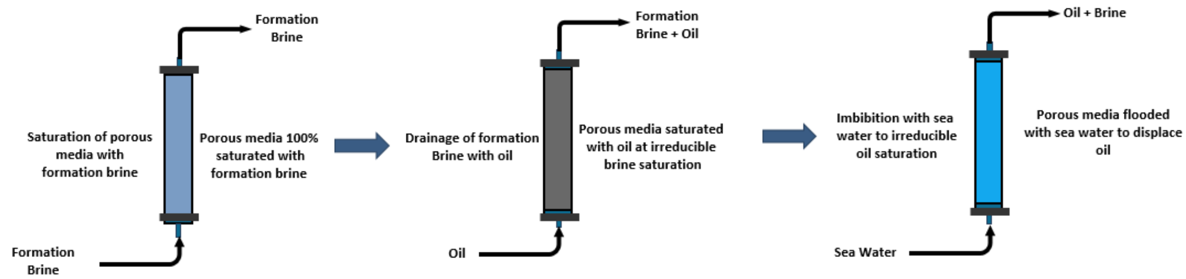

Figure 5: Schematic representation of the experimental flooding sequence.

During each run, produced effluent was collected in 50 cm^3 graduated cylinder of 1-inch diameter for separation of oil and water and subsequent material balance calculations performed. Small diameter measuring cylinders were used to minimise error. The graduated cylinders were changed every time period with longer periods at the beginning of the flood because there was little production. The rate of changing the cylinders was increased at water break-through, which was the peak of oil production. After this period, the effluent collection frequency was reduced. The time and cylinder number were recorded at each time-step when the cylinders were changed and mapped with the pressure log time in the LabVIEW program.

Due to the emulsion formation of the produced effluent, the weighting method was not feasible for accurate readings. In order to measure the recovered effluents, the measuring cylinders containing the effluents were placed in the convection oven at a temperature of 40 ^{o}C for 6 hours and allowed to separate for over 48 hours after which the respective phase volumes were recorded. This was used in computing the cumulative displaced fluid volumes. The dead volumes of the flow lines in the setup were measured and accounted for in all material balance calculations.

3.0 Relative permeability calculations

Relative permeability was computed through history matching with a commercial core flooding numerical simulator – Sendra. The software is a fully implicit 2-phase one dimensional black-oil simulation for analysing data from special core analysis experiment. It can be implemented for all common experimental approaches including both steady and unsteady-state flow experiments, single and multispeed centrifuge, as well as porous plate experiments. The software can be applied for either oil-water experiments, gas-oil or gas-water flow, during both imbibition and drainage processes.

History matching has been accepted as a standard approach for the estimation of oil-water relative permeabilities in the oil industry for many years (Barroeta and Thompson, 2006). History matching is an optimisation problem which requires tuning of the relative permeability curves until the computed differential pressure and the water/oil production volumes from numerical simulation are fitted to the experimental data (Kerig and Watson, 1986; Mitlin et al., 1998). Therefore, an appropriate objective function needs to be defined which in this case is a measure of the deviation between the measured or experimental and simulated data. The history matching process is thus aimed at minimising the objective function of the form of J in Eq. 3.

$$J = \left[\vec{Y} - \vec{F}(\vec{\beta})\right]^{T} W \left[\vec{Y} - \vec{F}(\vec{\beta})\right], \qquad 3$$

With respect to $\vec{\beta}$, with $\vec{\beta}$ been a (mX1) vector of the unknown parameters to be estimated, $\vec{Y}$ is a (nX1) vector of the measured data, W is a (nXn) weighting matrix, where each entry is set to the variance of the experimental data, and $\vec{F}(\vec{\beta})$ is a (nX1) vector of data values calculated from the mathematical model of the experimental process (Kerig and Watson, 1986).

Several optimisation techniques have been implemented for minimising the objective function during history matching procedure. The most commonly used are the Davidon-Fletcher-Powell (DFP), Fletcher-Reeves (FR), Quasi-Newton Approximation (QNA) and the Levenberg-Marquardt (LM) (Barroeta and Thompson, 2006). The LM method has been implemented in the Sendra software used for this study as it has been reported to function better than most of the other methods and completes the computation in the shortest time period (Savioli and Susana Bidner, 1994).

The recommended procedure for relative permeability estimation of displacement experiments is to start with the simplest correlations and to proceed to the more flexible correlations until the experimental data is history matched adequately (Sendra, 2018). While it is possible to optimise all the operating parameters in the history matching process, it is sufficient to optimise only the uncertain variables. Thus, the irreducible water saturation (S_{wi}) and oil relative permeability (K_{ro}) at irreducible water saturation has not been optimised as it is assumed that the K_{ro} is 1 at S_{wi}. Only the oil and water exponents and endpoint relative permeabilities have been optimised in this study.

For the history matching process, different relative permeability correlations such as Corey, LET, Burdine, Sigmund and McCaffery and Chierici were used to derive the best fit to the experimental data with the Corey and LET showing the closest fit and thus implemented. The Corey and LET models implemented in this study is consistent with previous related studies of Mitlin et al.(1998) , Ashrafi et al. (2014) and Esmaeili et al. (2019b). A short review of the different relative permeability models included in the Sendra simulator is given in the following section. In all of the models implemented, the same equation is used for the normalised water saturation as presented in Eq. 4.

$$S_w^* = \frac{S_w - S_{wi}}{1 - S_{wi} - S_{or}} \tag{4}$$

Corey Correlation

The popular and widely accepted Corey models (Eq. 5 and 6) were derived from the capillary pressure concept and has been widely applied for consolidated porous medium (Corey et al., 1956).

$$K_{rw} = K_{rw}^o\left({S_w^*}^{N_w}\right) \tag{5}$$

$$K_{ro} = K_{ro}^o(1 - S_w^*)^{N_o} \tag{6}$$

Where N_w and N_o are the water and oil Corey parameters respectively which shows the curvature of water and oil relative permeability curves.

LET Correlation

In Eq. 7 and 8, the parameters *L*, *E* and *T* are empirical. While L describes the shape of the curve in the lower parts, E describes the slope of the curve and the parameter T alters the top of the curves (Lomeland et al., 2005).

$$K_{rw} = K_{rw}^o \frac{(S_w^*)^{L_w}}{(S_w^*)^{L_w} + E_w(1 - S_w^*)^{T_w}} \tag{7}$$

$$K_{ro} = K_{ro}^o \frac{(1 - S_w^*)^{L_o}}{(1 - S_w^*)^{L_o} + E_o(S_w^*)^{T_o}} \tag{8}$$

4.0 Results and discussion

In this study, eighteen (18) different experiments were carried out to investigate the effect of temperature on relative permeability. All the experiments involved a displacement flow performed at varying temperature of 40, 60, and 80 °C with varying injection flow rates of 0.0083, 0.0125, and 0.0167 cm^3/s. Two different oil samples of varying viscosities and densities were used. A relatively low flow rate was chosen so as to mimic flow in a typical petroleum reservoir and all injection fluids are at ambient temperature. Table 5 and Table 6 summarise the experimental conditions considered for the study and correlation parameters used for the history matching of experimental data. Since the porous media is highly permeable, capillary pressure was not considered in the models.

4.1 Data treatment

Grubb's test (Grubbs and Beck, 1972) was used to assess the measured irreducible water saturation (S_{wi}), pore volume (PV) and calculated absolute permeability for outliers with a 95% confidence level. Figure 6 shows two outliers for the porous media pore volume while the permeability and initial water saturation contains no outlier from the Grubbs test conducted. Further statistical analysis of the results shows a normal distribution for the vast majority of the datasets.

Studies have shown that measurements taken on the same test setup could have a huge spread caused by several factors such as instrument uncertainty, material uncertainty and human errors. In this set of experiments, it is expected that error propagation would occur from the measured variables and ultimately result in some uncertainty in the calculated permeability. While the errors need to be quantified, Gommer et al. (2009) stated that overestimation of accuracy of the test setup and experimental error can cause a major effect on the calculated permeability due to error compounding. For our permeability calculations, only the instrument errors (differential pressure and injection flow rate) have been quantified and resultant uncertainties captured. Since both instruments have a no zero error, the uncertainty for each reading was estimated as half of the resolution of the instrument. Therefore, uncertainty values of ±0.00005 atm and 0.0005 cm^3/s for the differential pressure and flow rate respectively were taken as the errors propagated to the permeability calculations. For more detailed information on error propagation and uncertainty analysis, the reader is referred to Gommer et al. (2009) and Bodaghia et al. (2014).

To reduce the error for the porous media volume measurements, three attempts were made, and the average used. To find an estimate of the uncertainty of the averaged pore volume value for each system, the mean absolute error was used, calculated as absolute difference between the mean value and each measurement divided by the number of readings. Results of the pore volume and errors are presented in Table 5 and Table 6.

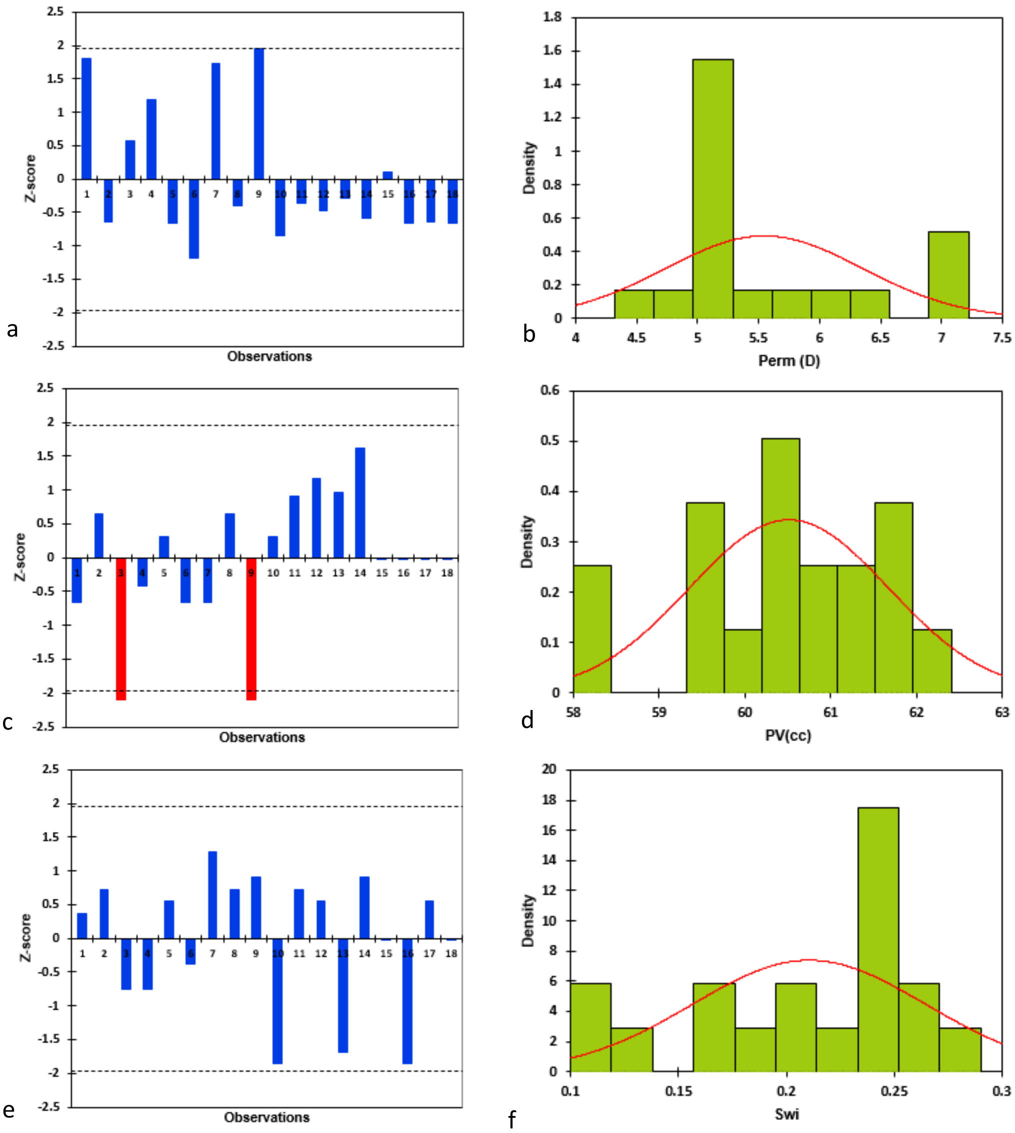

Figure 6: Z-score charts showing the outliers from Grubbs test (a. permeability, b. pore volume, c. initial water saturation) and histogram showing the normal distribution of the datasets (b. permeability, d. pore volume, f. initial water saturation).

Table 5: Specification of media properties and flow parameters in the series of experiments at 40 ^{o}C and Corey exponents used for the history matching.

S/N	Media permeability (K)	Pore volume (cm^3)	Porosity (%)	Initial water saturation (S_{wi})	Injection rate (cm^3/s)	Corey exponents	
						N_w	N_o
1	7.01 ± 0.48	59.75 ± 0.74	30.43 ± 1.24	0.23	0.0167	3.83	6.00
2	5.03 ± 0.38	61.26 ± 1.23	31.20 ± 2.01	0.25	0.0125	6.88	3.56
3	6.01 ± 0.75	58.09 ± 0.87	29.58 ± 1.50	0.17	0.0083	2.64	12.78
4	6.50 ± 0.43	60.02 ± 1.57	30.57 ± 2.61	0.17	0.0167	3.81	2.98
5	5.02 ± 0.38	60.88 ± 0.69	31.01 ± 1.14	0.24	0.0125	7.02	7.99
6	4.59 ± 0.50	59.75 ± 0.38	30.43 ± 0.64	0.19	0.0083	5.77	3.94

Table 6: Specification of media properties and flow parameters in the series of experiments at 60 and 80 ^{o}C and LET parameters used for the history matching.

S/N	Media permeability (K)	Pore volume (cm^3)	Porosity (%)	Initial water saturation (S_{wi})	Injection rate (cm^3/s)	LET parameters					
						L_w	E_w	T_w	L_o	E_o	T_o
7	6.95 ± 0.47	59.75 ± 0.55	30.43 ± 0.92	0.28	0.0167	1.52	2.28	0.8	4.26	6.29	0.82
8	5.23 ± 0.41	61.26 ± 0.74	31.20 ± 1.21	0.25	0.0125	5.38	0.55	0.8	3.8	4.37	0.78
9	7.12 ± 0.98	58.09 ± 0.57	29.58 ± 0.99	0.26	0.0083	1.96	2.63	0.8	5.43	7.91	0.87
10	4.86 ± 0.27	60.88 ± 0.92	31.01 ± 1.51	0.11	0.0167	1.89	2.39	0.8	4.26	7.74	0.87
11	5.25 ± 0.41	61.56 ± 0.93	31.35 ± 1.51	0.25	0.0125	1.89	2.39	0.8	4.26	7.74	0.87
12	5.17 ± 0.60	61.87 ± 0.54	31.51 ± 0.88	0.24	0.0083	3.05	1.15	0.8	4.77	13.85	0.58
13	5.32 ± 0.31	61.64 ± 1.08	31.39 ± 1.75	0.12	0.0167	5.00	3.99	0.8	5.00	1.49	0.98
14	5.07 ± 0.39	62.39 ± 0.01	31.77 ± 0.02	0.26	0.0125	3.05	3.69	1.34	3.85	29.8	1.66
15	5.63 ± 0.68	60.50 ± 0.79	30.81 ± 1.31	0.21	0.0083	2.39	3.42	0.95	2.31	45.9	1.59
16	5.02 ± 0.29	60.50 ± 1.78	30.81 ± 2.95	0.11	0.0167	7.20	1.12	0.8	2.47	5.54	0.63
17	5.03 ± 0.38	60.50 ± 1.13	30.81 ± 1.87	0.24	0.0125	5.00	1.77	0.8	6.50	1.40	0.65
18	5.01 ± 0.57	60.50 ± 0.99	30.81 ± 1.64	0.21	0.0083	7.49	0.37	0.89	3.96	8.00	0.59

Figure 7 shows sample results for the history matched and experimental data for differential pressure and corresponding cumulative oil production as a percentage of original oil in place (OOIP) against number of pore volume injected obtained. As seen from the figures, a good match was achieved between the experimental and simulated data in all the tests conducted in this study. In the history matching process, different relative permeability correlations were used, and the optimisation parameters estimated by the software to get the best match.

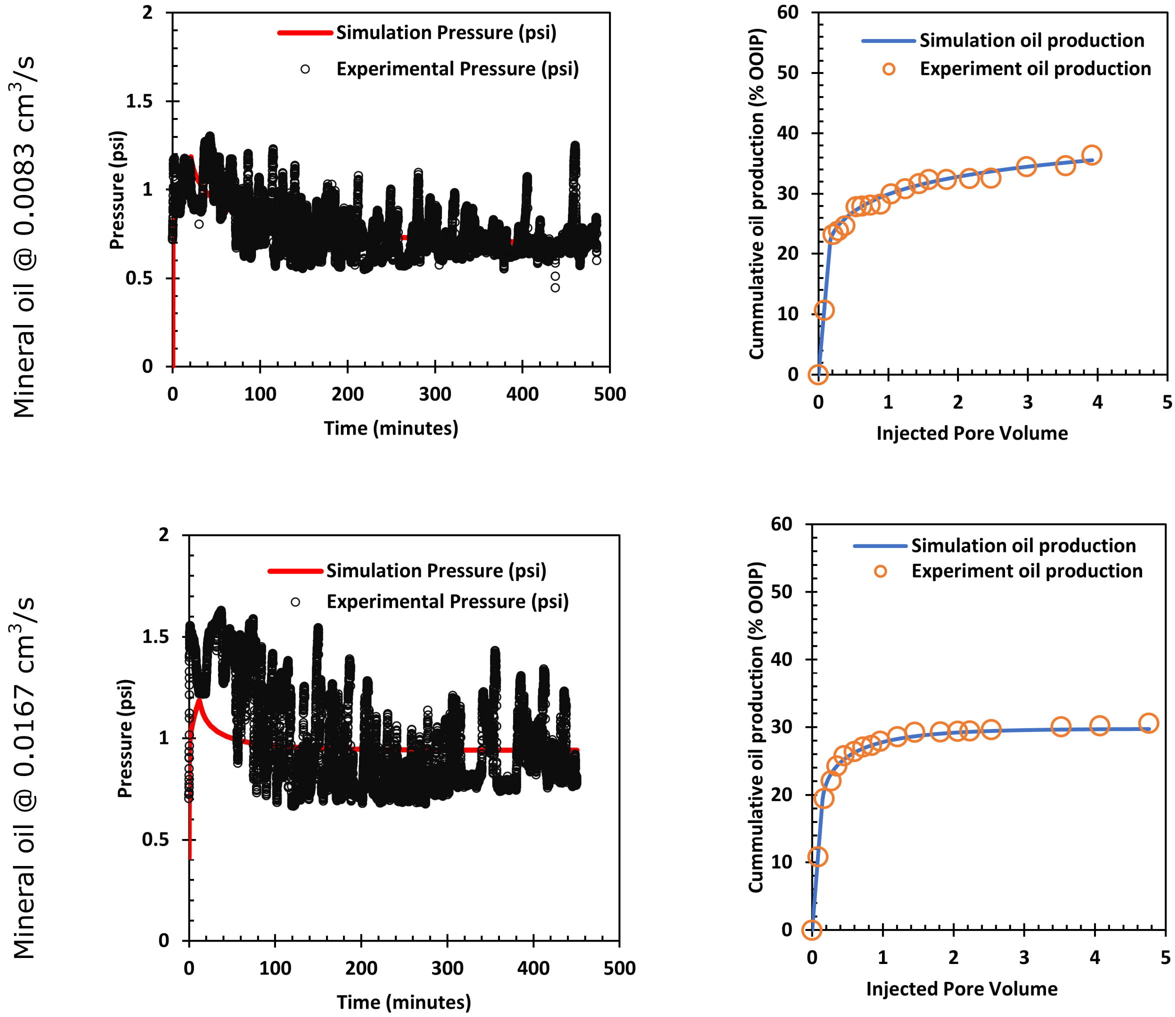

Figure 7: Experimental pressure data compared with history matched pressure from simulations (column 1). Experimental cumulative oil produced as a percentage of the OOIP against number of injected pore volume of water, compared with the production from history matched simulations corresponding to the pressure curve conditions under same condition as the pressure profiles (column 2).

4.2 Effect of temperature on irreducible water saturation and residual oil saturation

Plots of irreducible water and residual oil saturation with temperature are presented in Figure 8. In some experimental runs, a minor increase with temperature appears particularly from 40 to 60 °C. The low irreducible water saturation at low temperature is the result of the piston-like displacement scenario when a less viscous phase (water) is displaced by a more viscous phase (oil). With a rise in temperature, the viscosity of the oil reduces while the rock expands which reduces the micro-pores and blocks the pore throats making it difficult to displace the fluid filling the small pores. In addition, the reduction in viscosity at high temperature resulted in less efficient displacement at a given number of pore volumes injected. With a decrease in the oil viscosity, the viscosity ratio of oil to water decreases with an increase in the mobility ratio, leading to an increased flowability of the oil phase as a displacing phase thereby increasing the irreducible water saturation. A similar phenomenon is reported by Qin et al. (2018) who reported a linear increase in irreducible water saturation from 31.34 % at 45 °C to 39.31 % at 200 °C with an average increase of 2.66 % per 50 °C.

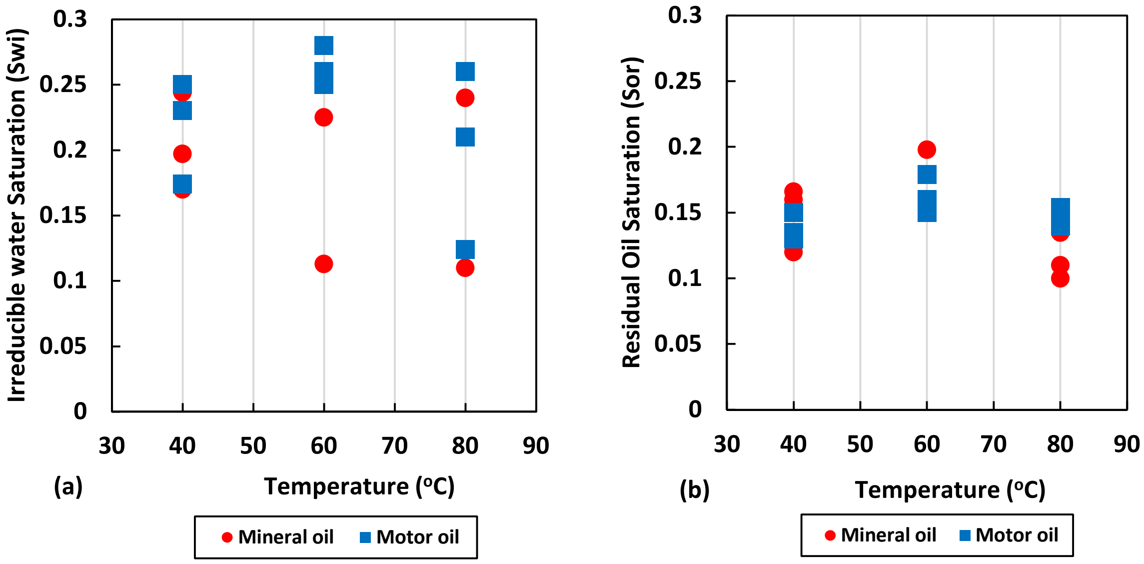

Figure 8: Plot of irreducible; (a) water saturation and (b) residual oil saturation for all the experiments conducted.

The result from the set of experiments conducted did not fully establish the trend of the irreducible water saturation increase with temperature as some fluctuations occurred when the temperature increases to 80 °C. The fluctuations in the results reflect the complex interplay of both the fluid viscosity ratio and injection flow rate at varying temperature conditions. This could potentially result in the occurrence of viscous fingering at low temperature as the water struggles to displace the more viscous oil phase. This phenomenon also accounts for the reason why the water cut increases rapidly after breakthrough. Under the present mobility ratio, it is apparent that viscous fingering seems to be inevitable. Droplets of oil occupying small pores within the porous matrix cannot be displaced, resulting in higher residual oil saturation. With a rise in temperature, the viscosity of the oil phase decreases, thereby decreasing the mobility ratio of water to oil. This occurrence reduces the effect of viscous fingering and results in a corresponding increase in the sweep area of water, thereby producing more oil at the outlet.

4.3 Effect of temperature and flow rate on production profile

Experimental data plots of cumulative oil production against number of injected pore volumes of water are shown in Figure 9. The data represents six (6) separate experiments with the motor oil under injection rate of 0.0083 and 0.0125 cm^3/s and temperatures of 40, 60, and 80 ^oC. In general, the curve begins to plateau after about one pore volume injected indicating the time of water breakthrough of approximately 1 hour. As shown in the figures, some disparity in the total production curves exist because the volume of injected water tends to vary with time along with small variations in the permeability of the sandpack. Due to the time constraint for each experimental flood, the residual oil saturation (S_{or}) was not attained. Therefore, S_{or} was included as one of the matching parameters in the Sendra software. The simulator in the history matching process could adjust the parameter freely. From the values output by the simulator, it is obvious that further water injection will not increase the ultimate recoveries significantly.

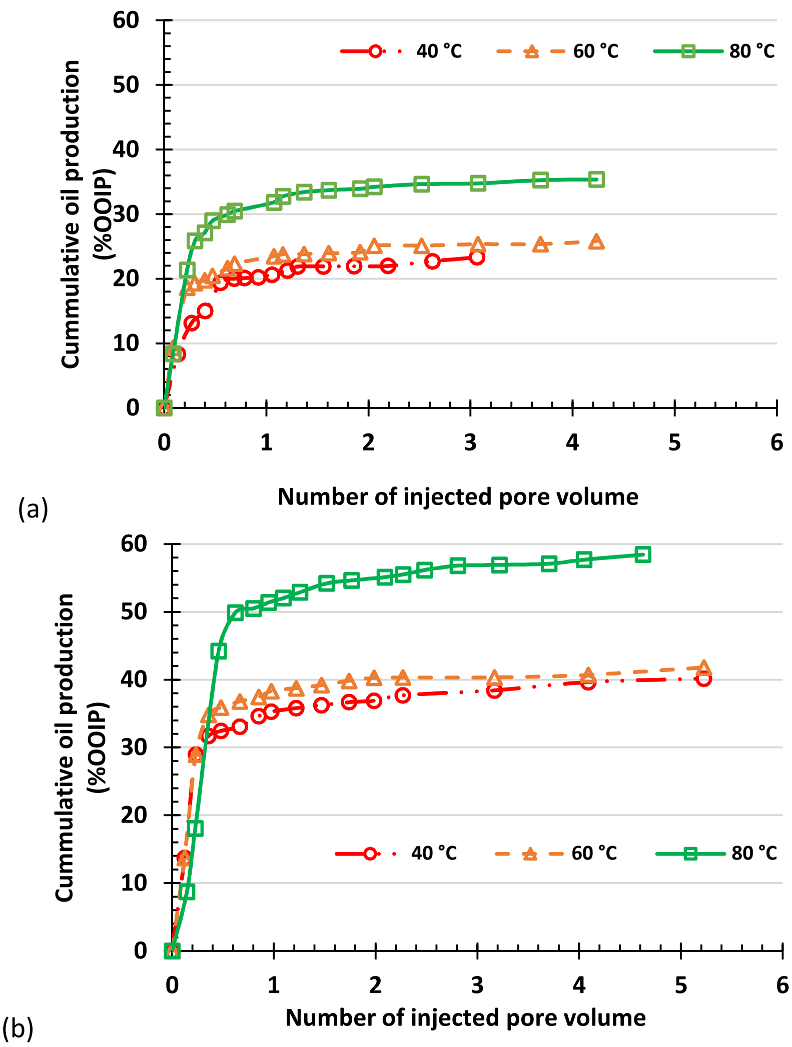

Figure 9: Cumulative oil production vs pore volumes injection for experimental runs on Motor oil at (a) 0.0083, and (b) 0.0125 cm^3/s under varying temperatures.

The initial water saturation (S_{wi}) for the range of experiments has an average of 0.21 with an average permeability of 5.55 mD. The flooding of the motor oil saturated sandpacks at 0.0083 cm^3/s recovered approximately 20–35% of OOIP for the different temperatures considered. As expected, the highest water flood recovery was attained at the highest temperature of 80 °C with a higher water/oil viscosity ratio. Our observation shows that a change in the operating temperature results in a significant difference in the recovery profile at 80 °C. This is apparently due to the favourable displacement owing to the fact the oil viscosity reduces with temperature, water/oil viscosity ratio increases and thereby favours the displacement of the oil by injected water. Although the temperature varies by 20 °C, the recovery profile between 40 to 60 °C shows an increase of about 14% compared to the 40 % increase from 60 to 80 °C. This is indicative of the fact that at 60 °C, an optimum flow condition has not been reached making it necessary to increase the temperature for increased recovery. The results show that with an increase in the operating temperature, the recovery increases by a factor of 58, 42, and 38 % at temperatures of 80, 60, and 40 °C respectively after 5 pore volumes were injected.

4.4 Effect of varying temperature on oil-water relative permeability curves

The relative permeability curves for the experiments performed on the unconsolidated sandpacks using motor and mineral oil at 0.0083 cm^3/s are shown in Figure 10. The plots show that there is a definite temperature dependency of both the oil and water relative permeability curves, though with varying magnitude. The difference in the oil-water relative permeability curves is noticeably larger for the mineral oil when compared to the motor oil under the same flow rate and operating temperature. This suggests that relative permeability sensitivity is significant to the mineral oil but very small compared to the water phase when the invading fluid phase was injected at 0.0083 cm^3/s. As seen for the mineral oil results, the effect of temperature on both the oil and water phase is pronounced with a shift to right as temperature increases. However, with an increase of the oil phase viscosity to a more viscous oil, while a similar result of temperature sensitivity is observed for the oil phase, the water shows insignificant variation making it apparent that the viscosity of the displaced fluid equally affects the curve.

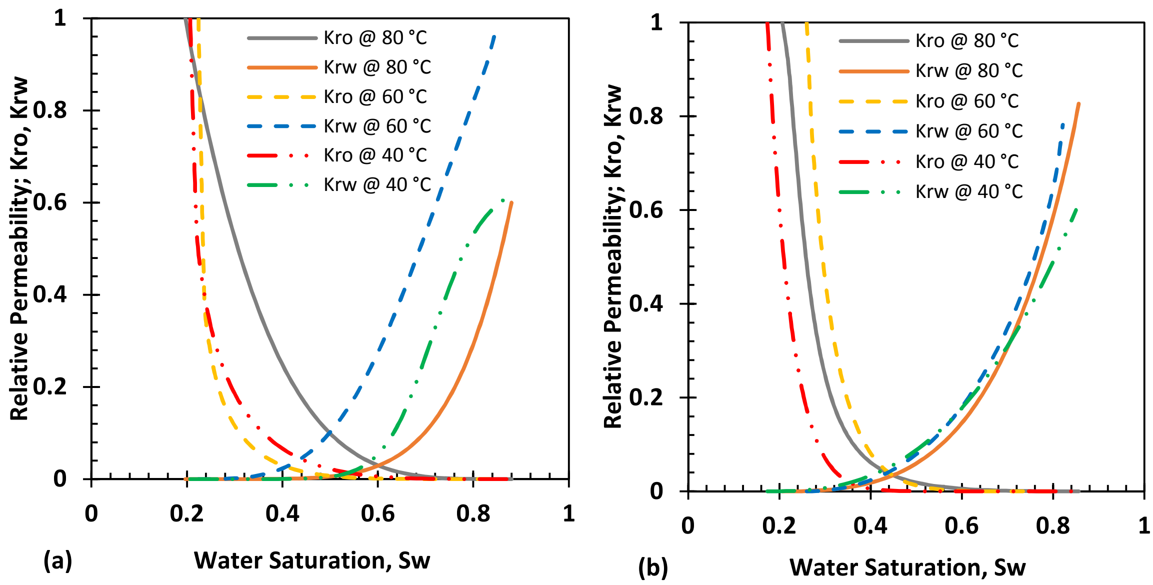

Figure 10: Relative permeability curves derived from implicit history matching of the experimental data with the simulator at 0.0083 cm^3/s for (a) mineral oil, and (b) motor oil.

Generally, oil and water relative permeability sensitivity to temperature is governed by three mechanisms, which are change in fluid viscosity, thermal expansion of porous matrix and fluid, coupled with the possible adsorption and desorption of fluid molecules. As the operating temperature increases, the oil viscosity decreases thereby enhancing the flow capability of oil. Furthermore, as the temperature increases, the adsorption of water molecules becomes stronger resulting in a decline of the mobility of water. Consequently, the oil phase has a higher relative increase in relative permeability when compared to the water phase. In addition, the thermal expansion of the rock matrix and fluid triggered by the increase in temperature creates an expansion pressure that acts as a drive mechanism and support the production of fluid. This pressure results in a corresponding increase in the oil-water relative permeability.

The observed phenomena could be explained in terms of fundamental multiphase flow concepts involving wettability and contact angles. According to Tarek (2019) there exists two main distinguishing features between oil-wet and water-wet relative permeability curves. Firstly, if the crossover saturation, that is the water saturation at which oil and water relative permeability curves are equal or intersects is greater than 50 %, the media is a water-wet system. On the other hand if it is less than 50 % it is an oil-wet system. The relative permeability curves shown in Figure 11 for both mineral and motor oils under varying temperatures can be explained based on the wettability condition of the porous sandpacks.

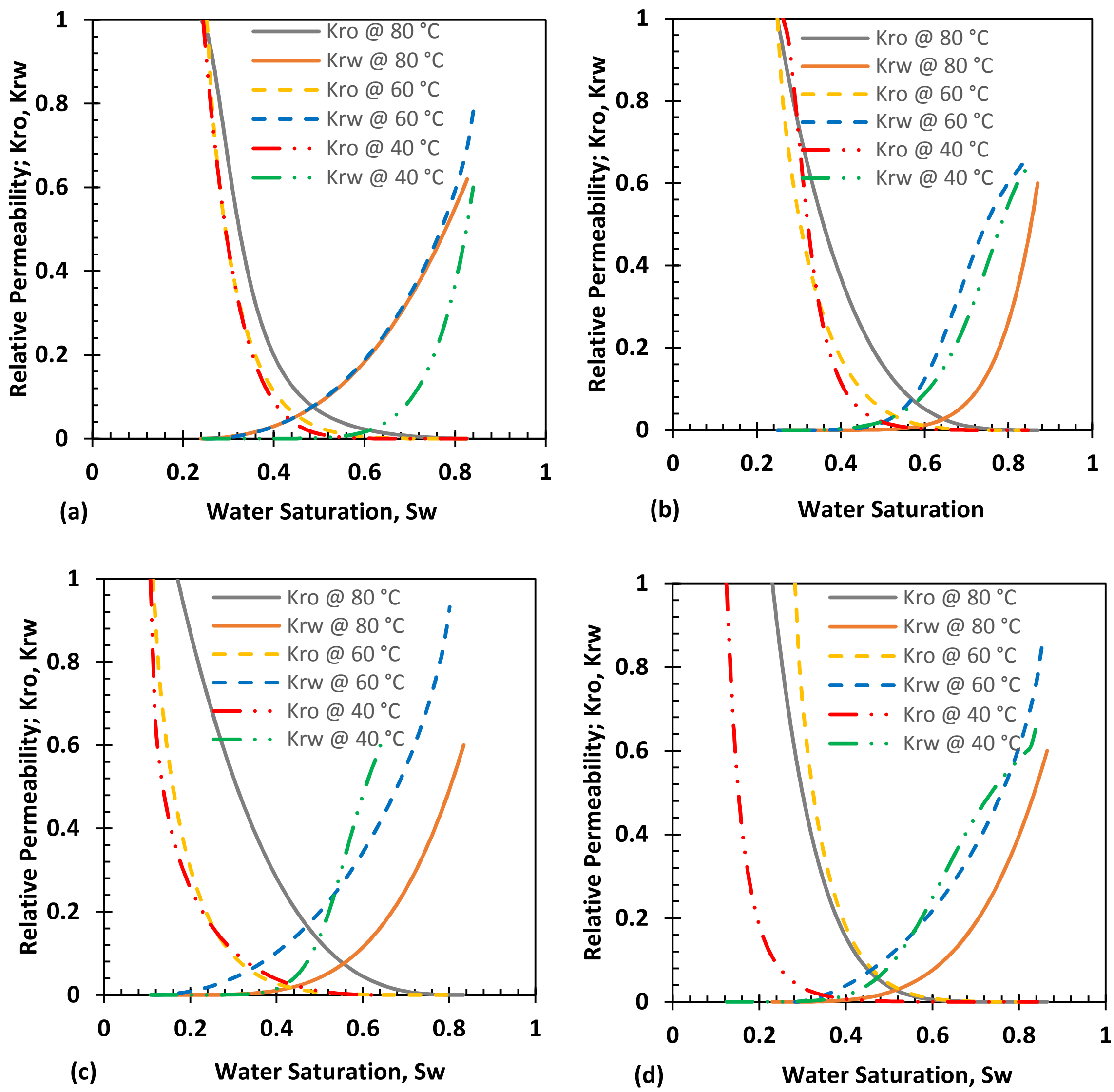

Figure 11: Relative permeability curves derived from implicit history matching of the experimental data with the simulator at (a) mineral oil – 0.0125 cm^3/s, (b) motor oil - 0.0125 cm^3/s, (c) mineral oil – 0.0167 cm^3/s, and (d) motor oil – 0.0167 cm^3/s.

The presented relative permeability curves show that with an increase in temperature, the water saturation at crossover points increase nonlinearly, particularly at the temperature of 80 °C. At 40 °C, with an injection of 0.0125 cm^3/s for motor oil, the water saturation at crossover point is about 44.45 %, and it reaches 65.20 % at 80 °C (Figure 11 b). A similar trend is observed at flow rate of 0.0167 cm^3/s at 80 °C with a crossover saturation being 58.5 % and 53.55 % for mineral and motor oil respectively (Figure 11 c & d). It is apparent that the water-wetness of the media is supported at high temperature for most of the systems. The change of wettability shows that elevated temperature results in adsorption of fluid molecules and alteration of rock properties. The water saturation at crossover or equal-permeability points shows a gradual increase as the temperature increases. This is reflected in the variations in residual oil saturations and permeability endpoints. The experimental results presented has been able to demonstrate the effect of temperature on relative permeability curves.

4.5 Empirical Model development

Relative permeability values evaluated under typical reservoir temperature and pressure are deemed reliable and representative of the real-world situation. However, this approach is fundamentally time expending, complex, and expensive. Consequently, empirical correlations, and mathematical models have been formulated from an abundance of experimental data to compute oil-water relative permeability. Relative permeability values generated from empirical models have been found to have agreeable comparison with experimental data, however, many of these mathematical models do not consider the effect of temperature (Xiao et al., 2012; Xu et al., 2013; Mahon et al., 2020). In recent years, several empirical models have been developed with the temperature effect included but among the several models, that of Zhang (2017) is the most reliable (Esmaeili et al., 2019a; Menad et al., 2019). The Zhang model has therefore been adopted and appropriately adapted for this study.

The Zhang model was formulated utilising experimental data gathered from temperature dependent oil-water relative permeability. The unsteady-state experimental method was carried out using tight sandstone with light oil of viscosity range; $4 \leq \mu_o \leq 48\, cP$ under a temperature range; $25 \leq T \leq 100^oC$. In developing the model, the authors used a combination of JBN and Corey correlation with a set of empirical constants that can be adopted to fit experimental data generated under real reservoir conditions.

While empirical models are simple and easy to use, they are not capable of making accurate predictions under conditions different from those for which they were developed (Fan et al., 2019). Since the operating conditions under which the model was formulated falls outside the range of parameters for this study, modifications were made to adopt the model. For this purpose, a nonlinear least squares regression was implemented to fit the Zhang model to our experimental dataset. This approach was chosen as it can be used with a large and more general class of functions. While a nonlinear least square regression has the advantage of producing reliable results with limited data sets, a major challenge is the need to supply initial guess values for the unknown parameters prior to the optimisation process. It is expected that the initial values be moderately close to that of the unknown parameter for the optimisation procedure to converge (NIST/SEMATECH, 2013).

The Zhang model is presented in its original form, Eq. 9 and 10, while the empirical constants have been optimised using the nonlinear least square method for application with unconsolidated porous media; sandpacks or glass beads, for a similar temperature range and oil viscosity.

$$k_{rw} = k_{rw-50}^{o}(e_1 + e_2 T + \frac{e_3}{T} + \frac{e_4}{T^2})\left(\frac{S_w - S_{wi}}{1 - S_{wi} - S_{or}}\right)^{a_3 T + a_4} \tag{9}$$

and

$$k_{ro} = \left(\frac{1 - S_w - c_1 \ln(T) - c_2}{1 - b_1 T - b_2 - c_1 \ln(T) - c_2}\right)^{a_1 T + a_2} \tag{10}$$

Specifically, for the unconsolidated sandpacks used in our experiments and porous media of similar nature, the optimised values of the empirical parameters in the Eq. 9 and 10 above are as follows: a_1=-0.00295, a_2=3.976, a_3=-9.9991E-06, a_4=4.176, b_1=0.0025, b_2=0.001, c_1=-0.1121, c_2=0.6711, e_1=20.14, e_2=-0.053, e_3=-1638.84, e_4=40763.24, k_{rw-50}^{o}=0.048.

Comparison of our experimental relative permeability and the empirical correlation result is presented in Figure 12. The results show that the oil and water relative permeability values generated from the empirical model adapted to fit the experiment data and optimised constants compares well with the experimental values. The predicted results compare well with experimental data with a variance of 0.08175 and 0.0055 for oil and water respectively, a root mean square error value of 0.01 and R^2 of 0.994 for the oil phase and root mean square error of 0.02 and R^2 of 0.975 for water.

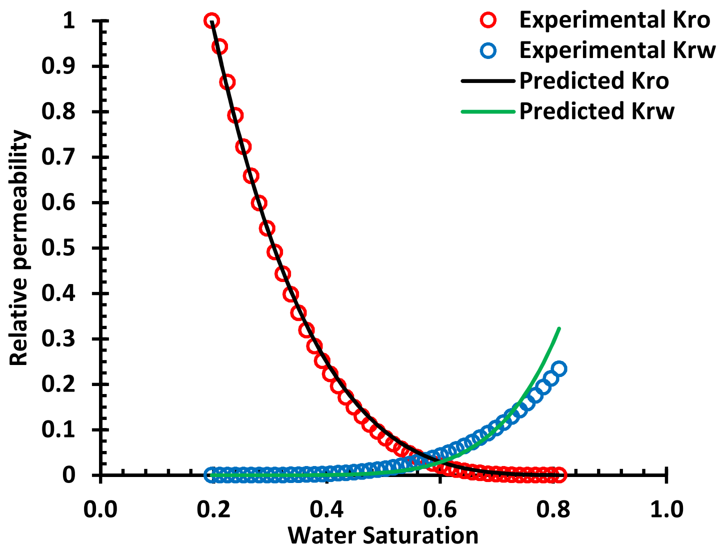

Figure 12:Comparison between the relative permeability curves derived from implicit history matching of the experimental data with the simulator and outputs predicted from the empirical model with the modified empirical constants.

4.5.1 Model validation

Figure 13 is a validation plot to evaluate the reliability of the optimised parameters in use with the Zhang correlations for predicting temperature dependent oil-water relative permeability in unconsolidated porous media. Experimental data from Ashrafi et al. (2012) using light oil and glass beads of relative high permeability at 70 °C has been compared with relative permeability values generated from the empirical model. As seen in Figure 13, relative permeability values generated from the empirical model compare satisfactorily with data from published experimental data in literature with a variance of 0.11211 and 0.00024 for oil and water respectively, establishing the reliability of the predictive capability of using the optimised constants with the Zhang model in literature.

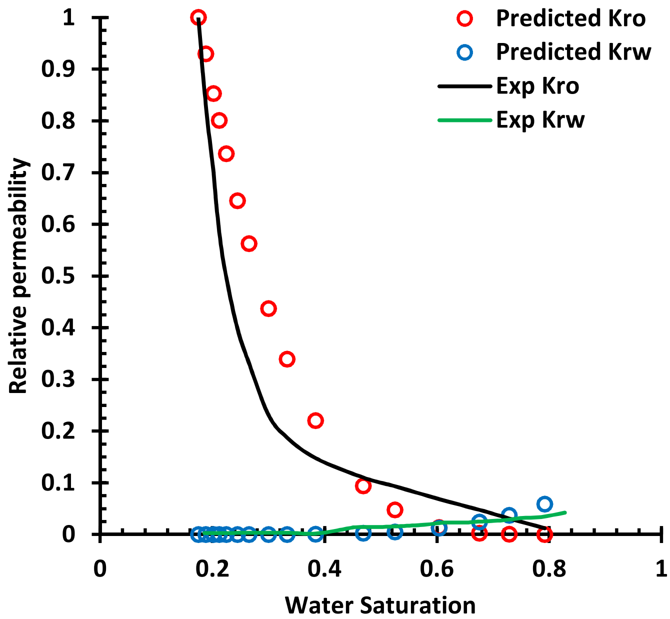

Figure 13: Comparison between experimental relative permeability from Ashrafi et al., (2012) and outputs generated the modified empirical constants in this study.

It should be noted that the proposed empirical constants with the model for predicting a temperature dependent oil and water relative permeability needs to be used when the operating conditions fall within the range of applicability, otherwise its reliability is not guaranteed.

5.0 Conclusion

In this study, the effect of temperature on oil-water relative permeability curves has been investigated for a set of unconsolidated sandpack porous systems. The unsteady-state water flood method was adopted and numerical computation with history matching implemented for the analysis of experimental data and generation of relative permeability curves. Generated experimental data was curated and used to derive a set of empirical constants to be used with relative permeability correlations.

Based on the results and discussion presented, the following conclusions can be drawn on the effect of temperature on oil-water relative permeability of porous sandpacks.

- A general trend for the series of experiments conducted shows an increase in the oil and water relative permeabilities occasioned by a rightward shift of the curves with rising temperature. In addition, the irreducible water saturation increased with a rise in temperature, coupled with a decrease in the residual oil saturation in most of the experimental runs.
- With a rise in temperature is the rightward shift of the crossover saturation beyond 0.5 of the water saturations, indicative of a shift to water-wetness with temperature increase. The influence of viscous fingering and unstable displacement front due to an adverse mobility ratio condition is apparent in the results owing to the viscosity ratio and media properties.
- The shape of oil relative permeability curves for sandpack systems with a highly viscous oil increased with a rise in injection flow rate. An opposite trend was observed for the less viscous oil as an increase in the injection flow rate does not favour the displacement process. In other words, with increasing flow rate the relative permeability curves increases for more viscous oils and decreases for less viscous oils.
- The residual oil saturation is observed to be sensitive to the injection flow rate for both oil systems. The flooded sandpack with highly viscous oil shows a reducing value for the residual oil saturation with increasing flow rate. At intermediate flow rate considered, the residual oil saturation is unaffected, but a higher residual oil saturation was observed in the lighter oil under the same flow rate. With regards to the water relative permeability curves, the effect is minimal in most of the cases. With the general trend showing the highest water relative permeability curve under the highest flowing rate.
- The end-point water relative permeability varies slightly for the set of experiments with the values being higher for the less viscous oil under the same flow rate. The effect of oil viscosity on fractional flow and consequently on the oil recovery was observed to be more predominant in the tests under higher flow rate and shows a higher fractional flow for the lighter oil.

In summary, the results presented in this study demonstrate that relative permeability curves are affected by the operating temperature, injection flow rate and fluid viscosity. Consequently, the temperature factor is a vital parameter to be considered when incorporating relative permeability data into reservoir simulators for effective reservoir production modelling.

References

Akhlaghinia, M., Torabi, F., Chan, C.W., 2014. Experimental investigation of temperature effect on three-phase relative permeability isoperms in heavy oil systems. Fuel 118. https://doi.org/10.1016/j.fuel.2013.10.049

Akin, S., Castanier, L.M., Brigham, W.E., 1998. Effect of temperature on heavy-oil/water relative permeabilities, in: SPE Annual Technical Conference and Exhibition. Society of Petroleum Engineers. https://doi.org/10.2118/49021-MS

Ali, J.K., 1997. Developments in measurement and interpretation techniques in coreflood tests to determine relative permeabilities, in: Latin American and Caribbean Petroleum Engineering Conference. Society of Petroleum Engineers. https://doi.org/10.2118/39016-MS

Archer, J.S., Wong, S.W., 1973. Use of a reservoir simulator to interpret laboratory waterflood data. Soc. Pet. Eng. J. 13. https://doi.org/10.2118/3551-PA

Ashrafi, M., Souraki, Y., Torsaeter, O., 2012. Effect of temperature on Athabasca type heavy oil – Water relative permeability curves in glass bead packs. Energy Environ. Res. 2. https://doi.org/10.5539/eer.v2n2p113

Ashrafi, M., Souraki, Y., Torsaeter, O., 2014. Investigating the temperature dependency of oil and water relative permeabilities for heavy oil systems. Transp. Porous Media 105. https://doi.org/10.1007/s11242-014-0382-8

Barroeta, R., Thompson, L.G., 2006. Estimation of relative permeability from displacement pressure data, in: SPE/DOE Symposium on Improved Oil Recovery. Society of Petroleum Engineers. https://doi.org/10.2118/99734-MS

Bodaghia, M., Gonçalves, P., Correiab, N., 2014. A quantitative evaluation of the uncertainty of permeability measurements in constant thickness fibre reinforcements (rtm), in: ECCM16 - 16th European Conference on Composite Materials. Seville, Spain, pp. 1–8.

Buckley, S.E., Leverett, M.C., 1942. Mechanism of fluid displacement in sands. Trans. AIME 146. https://doi.org/10.2118/942107-G

Cao, L., Li, S., 2016. The effect of temperature and rock permeability on oil-water relative permeability curves of waxy crude oil. Int. J. Eng. Res. Appl. 6, 16–21.

Closmann, P.J., Waxman, M.H., Deeds, C.T., 1988. Steady-state tar/water relative permeabilities in Peace River cores at elevated temperature. SPE Reserv. Eng. 3. https://doi.org/10.2118/14227-PA

Corey, A.T., Rathjens, C.H., Henderson, J.H., Wyllie, M.R.J., 1956. Three-phase relative permeability. J. Pet. Technol. 8. https://doi.org/10.2118/737-G

Esfahani, M.R., Haghighi, M., 2004. Wettability evaluation of Iranian carbonate formations. J. Pet. Sci. Eng. 42. https://doi.org/10.1016/j.petrol.2003.12.016

Esmaeili, S., Sarma, H., Harding, T., Maini, B., 2019. A data-driven model for predicting the effect of temperature on oil-water relative permeability. Fuel 236. https://doi.org/10.1016/j.fuel.2018.08.109

Esmaeili, S., Sarma, H., Harding, T., Maini, B., 2019. The effect of temperature on two-phase oil/water relative permeability in different rock/fluid systems, in: SPE Annual Technical Conference and Exhibition. Society of Petroleum Engineers. https://doi.org/10.2118/195859-MS

Fan, J., Wu, L., Zhang, F., Cai, H., Zeng, W., Wang, X., Zou, H., 2019. Empirical and machine learning models for predicting daily global solar radiation from sunshine duration: A review and case study in China. Renew. Sustain. Energy Rev. 100. https://doi.org/10.1016/j.rser.2018.10.018

Gommer, F., Lomov, S., Vandenbosche, K., Verpoest, I., 2009. Error assessment in permeability measurement using radial flow method. Adv. Compos. Lett. 18. https://doi.org/10.1177/096369350901800402

Grubbs, F.E., Beck, G., 1972. Extension of sample sizes and percentage points for significance tests of outlying observations. Technometrics 14. https://doi.org/10.2307/1267134

Hamouda, A.A., Karoussi, O., Chukwudeme, E.A., 2008. Relative permeability as a function of temperature, initial water saturation and flooding fluid compositions for modified oil-wet chalk. J. Pet. Sci. Eng. 63. https://doi.org/10.1016/j.petrol.2008.10.002

Hamouda, A., Karoussi, O., 2008. Effect of temperature, wettability and relative permeability on oil recovery from oil-wet chalk. Energies 1. https://doi.org/10.3390/en1010019

Honarpour, M., Mahmood, S.M., 1988. Relative-permeability measurements: An overview. J. Pet. Technol. 40. https://doi.org/10.2118/18565-PA

Johnson, E.F., Bossler, D.P., Bossler, V.O.N., 1959. Calculation of relative permeability from displacement experiments. Trans. AIME 216. https://doi.org/10.2118/1023-G

Jones, S.C., Roszelle, W.O., 1978. Graphical techniques for determining relative permeability from displacement experiments. J. Pet. Technol. 30. https://doi.org/10.2118/6045-PA

Kerig, P.D., Watson, A.T., 1986. Relative-permeability estimation from displacement experiments: An error analysis. SPE Reserv. Eng. 1. https://doi.org/10.2118/12589-PA

Klinkenberg, L.J., 1941. The permeability of porous media to liquids and gases, in: Drilling and Production Practice. American Petroleum Institute, New York.

Kovscek, A.R., Vega, B., 2014. Steady-state relative permeability measurements, temperature dependency and a reservoir diatomite core sample evolution, in: SPE Annual Technical Conference and Exhibition. Society of Petroleum Engineers. https://doi.org/10.2118/170918-MS

Kumar, M., Inouye, T.A., 1994. Low-temperature analogs of high-temperature water/oil relative permeabilities, in: SPE Annual Technical Conference and Exhibition. Society of Petroleum Engineers. https://doi.org/10.2118/28616-MS

Kumar, S., Torabzadeh, S.J., Handy, L.L., 1985. Relative permeability functions for high- and low-tension systems at elevated temperatures, in: SPE California Regional Meeting. Society of Petroleum Engineers. https://doi.org/10.2118/13670-MS

Lenormand, R., Lorentzen, K., Maas, J.G., Ruth, D., 2016. Comparison of four numerical simulators for SCAL experiments, in: International Symposium of the Society of Core Analysts. Snowmass, Colorado, pp. 1–12.

Lomeland, F., Ebeltoft, E., Thomas, W.H., 2005. A new versatile relative permeability correlation, in: International Symposium of the Society of Core Analysts. Toronto, Canada, pp. 1–12.

Mahon, R., Balogun, Y., Oluyemi, G., Njuguna, J., 2020. Swelling performance of sodium polyacrylate and poly(acrylamide-co-acrylic acid) potassium salt. SN Appl. Sci. 2. https://doi.org/10.1007/s42452-019-1874-5

Maini, B.B., Batycky, J.P., 1985. Effect of temperature on heavy-oil/water relative permeabilities in horizontally and vertically drilled core plugs. J. Pet. Technol. 37. https://doi.org/10.2118/12115-PA

Maini, B.B., Kokal, S., Jha, K., 1989. Measurements and correlations of three-phase relative permeability at elevated temperatures and pressures, in: SPE Annual Technical Conference and Exhibition. Society of Petroleum Engineers. https://doi.org/10.2118/19677-MS

Maini, B.B., Okazawa, T., 1987. Effects of temperature on heavy oil-water relative permeability of sand. J. Can. Pet. Technol. 26. https://doi.org/10.2118/87-03-03

Menad, N.A., Noureddine, Z., Hemmati-Sarapardeh, A., Shamshirband, S., 2019. Modeling temperature-based oil-water relative permeability by integrating advanced intelligent models with grey wolf optimization: Application to thermal enhanced oil recovery processes. Fuel 242. https://doi.org/10.1016/j.fuel.2019.01.047

Miller, M.A., Ramey, H.J., 1985. Effect of temperature on oil/water relative permeabilities of unconsolidated and consolidated sands. Soc. Pet. Eng. J. 25. https://doi.org/10.2118/12116-PA

Mitlin, V.S., Lawton, B.D., McLennan, J.D., Owen, L.B., 1998. Improved estimation of relative permeability from displacement experiments, in: International Petroleum Conference and Exhibition of Mexico. Society of Petroleum Engineers. https://doi.org/10.2118/39830-MS

NIST/SEMATECH, 2013. Emgineering Statistics e-Handbook of Statistical Methods [WWW Document]. URL https://www.itl.nist.gov/div898/handbook/ (accessed 6.13.20).

Oluyemi, G.F., 2014. Conceptual physicochemical models for scale inhibitor-formation rock interaction. Pet. Sci. Technol. 32. https://doi.org/10.1080/10916466.2011.580293

Polikar, M., Ali, S.M.F., Puttagunta, V.R., 1990. High-temperature relative permeabilities for Athabasca oil sands. SPE Reserv. Eng. 5. https://doi.org/10.2118/17424-PA

Qin, Y., Wu, Y., Liu, P., Zhao, F., Yuan, Z., 2018. Experimental studies on effects of temperature on oil and water relative permeability in heavy-oil reservoirs. Sci. Rep. 8. https://doi.org/10.1038/s41598-018-31044-x

Rostami, P., Mehraban, M.F., Sharifi, M., Dejam, M., Ayatollahi, S., 2019. Effect of water salinity on oil/brine interfacial behaviour during low salinity waterflooding: A mechanistic study. Petroleum 5. https://doi.org/10.1016/j.petlm.2019.03.005

Satter, A., Iqbal, G., Buchwalter, J.L., 2008. Practical Enhanced Reservoir Engineering: Assisted with Simulation Software. PennWell Books.

Savioli, G.B., Susana Bidner, M., 1994. Comparison of optimization techniques for automatic history matching. J. Pet. Sci. Eng. 12. https://doi.org/10.1016/0920-4105(94)90004-3

Schembre, J.M., Tang, G., Kovscek, A.R., 2005. Effect of temperature on elative permeability for heavy-oil diatomite reservoirs, in: SPE Western Regional Meeting. Society of Petroleum Engineers. https://doi.org/10.2118/93831-MS

Sendra, 2018. Sendra User Guide 2018.2. Norway.

Sola, B.S., Rashidi, F., Babadagli, T., 2007. Temperature effects on the heavy oil/water relative permeabilities of carbonate rocks. J. Pet. Sci. Eng. 59. https://doi.org/10.1016/j.petrol.2007.02.005

Sufi, A.H., Ramey, H.J., Brigham, W.E., 1982. Temperature effects on relative permeabilities of oil-water systems, in: SPE Annual Technical Conference and Exhibition. Society of Petroleum Engineers. https://doi.org/10.2118/11071-MS

Talreja, R., Kumar, R., Gupta, A., Behera, P.K., Munshi, B., 2020. Laboratory tests to evaluate the temperature effects on rock properties of sandstone rock, in: ARMA/DGS/SEG International Geomechanics Symposium. American Rock Mechanics Association, Virtual.

Tarek, A., 2019. Reservoir Engineering Handbook. Elsevier. https://doi.org/10.1016/C2016-0-04718-6

Torabzadey, S.J., 1984. The effect of temperature and interfacial tension on water/oil relative permeabilities of consolidated sands, in: SPE Enhanced Oil Recovery Symposium. Society of Petroleum Engineers. https://doi.org/10.2118/12689-MS

Watson, R.W., Ertekin, T., 1988. The effect of steep temperature gradient on relative permeability measurements, in: SPE Rocky Mountain Regional Meeting. Society of Petroleum Engineers. https://doi.org/10.2118/17505-MS

Xiao, B., Fan, J., Ding, F., 2012. Prediction of relative permeability of unsaturated porous media based on fractal theory and Monte Carlo simulation. Energy & Fuels 26. https://doi.org/10.1021/ef3013322

Xu, P., Qiu, S., Yu, B., Jiang, Z., 2013. Prediction of relative permeability in unsaturated porous media with a fractal approach. Int. J. Heat Mass Transf. 64. https://doi.org/10.1016/j.ijheatmasstransfer.2013.05.003

Zeidani, M., Maini, B.B., 2016. SAGD relative permeability as a function of temperature, in: SPE Canada Heavy Oil Technical Conference. Society of Petroleum Engineers. https://doi.org/10.2118/180713-MS

Zhang, L., Tong, J., Xiong, Y., Zhao, Y., 2017. Effect of temperature on the oil–water relative permeability for sandstone reservoirs. Int. J. Heat Mass Transf. 105. https://doi.org/10.1016/j.ijheatmasstransfer.2016.10.029

Table 1: Summary of literature reports on the effect of temperature on relative permeability.

	Reference	Materials		Method	Operating conditions		Effect of temperature on relative permeability
		Porous media	Fluid		Temperature (^{o}C)	Pressure (psi)	
1	Sufi et al. (1982)	Unconsolidated sandstone	Refined oil	USS (JBN and Welge)	Up to 149	2000	No effect
2	Torabzadeh and Handy (1984)	Berea sandstone	Dodecanese	USS and SS	$21 \leq T \leq 177$	650	K_{ro} increases and K_{rw} decreases
3	Miller and Ramey (1985)	Ottawa and Berea sands	Refined oil	-	$19 \leq T \leq 149$	500	No effect
4	Maini and Batycky (1985)	Sandstone	Heavy oil	USS, History matching	$25 \leq T \leq 272$	1100	Reduction in K_{ro} and K_{rw} remain unchanged
5	Kumar et al. (1985)	Berea sandstone Peace River sand	Dodecanese	Theoretical	Up to 177	-	K_{ro} increases and K_{rw} decreases K_r curve affected
6	Closmann et al. (1988)	Berea sandstone	Unaltered, thermally altered and deasphalted tar	SS	$62 \leq T \leq 169$	-	-
7	Watson and Ertekin (1988)	Ottawa silica	Refined oil	SS	$104 \leq T \leq 149$	-	Reduction of K_{ro} and K_{rw} due to formation of third Phase
8	Maini et al. (1989)	Berea sand	Refined oil	USS (history matching)	100	-	K_r curve affected
9	Polikar et al. (1990)	Athabasca sandstone	Heavy oil	SS and USS	$100 \leq T \leq 250$	-	No effect
10	Kumar and Inuouye (1994)	Unconsolidated sandstone	White, refined and heavy oil	USS (JBN)	$24 \leq T \leq 160$	-	-
11	Akin et al. (1998)	Ottawa sandstone and sandpack	Mineral oil	Simulation	$22 \leq T \leq 66$	-	No effect
12	Esfahani and Haghighib	Dolomite and limestone	Light oil	USS (JBN)	$16 \leq T \leq 104$	-	Increasing temperature makes rocks oil-wet

	(2004)						
13	Schembre et al. (2005)	Diatomite cores	Mineral and crude oil	USS	$120 \leq T \leq 180$	-	Media becomes more water wet with K_{rw} and K_{ro} affected by temperature
14	Sola et al. (2007)	Dolomite	Heavy oil	USS	$38 \leq T \leq 260$	2500	K_{ro} becomes more linear and K_{rw} reduces
15	Hamouda et al. (2008)	Chalk core sample	n-decane	Jones and Rosezelle	Up to 130	-	Kr shifts to right at about 80 ^oC as more water wet but shifts to oil wet state at about 130 ^oC
16	Hamouda and Karoussi (2008)	Chalk core samples	-	Simulation	$23 \leq T \leq 130$	-	Effects due to experimental artefacts
17	Ashrafi et al. (2014)	Unconsolidated sandpacks	Athabasca bitumen	USS History matching	Up to 300	363	K_r affected by temperature
18	Kovscek and Vega (2014)	Siliceous shale	Dehydrated dead oil	SS	$45 \leq T \leq 230$	-	K_{rw} shifts to the right as temperature increases
19	Akhlaghinia et al. (2014)	Consolidated sandstone core	Heavy oil	JBN method	$28 \leq T \leq 52$	-	K_{rw} and K_{ro} increases as temperature rises to about 40 ^oC, K_{ro} decreases when temperature reaches 52 ^oC
20	Zeidani and Maini (2016)	Unconsolidated sandpack	Athabasca reservoir oil	USS History matching	Up to 220	-	Residual oil saturation decreases with temperature
21	Cao et al. (2016)	Consolidated reservoir cores	Waxy crude oil	USS	$50 \leq T \leq 85$	-	K_{rw} and K_{ro} increases with temperature
22	Qin et al. (2018)	Unconsolidated sandpacks	Heavy oil	USS	$45 \leq T \leq 200$	-	-

Table 2: Physical properties of silica sand used for this study.

Typical physical properties of the sand sample	
Colour	White
Grain shape	Round
Hardness (Mohs)	7
Melting point (°C)	1710
Mineral	Quartz
Bulk density	1.68 g/cc
Specific gravity	2.65 g/cc
pH	7

Table 3: Physical properties of the fluid samples used for the experiments at ambient condition.

Fluid	**Density (kg/m3)**	**Viscosity (cP)**
Brine (SW)	1000	1.003
Brine (FW)	1020	1.005
Oil	850	147

Table 4: Chemical composition of the synthetic brine samples.

Salt (ppm)/Brine	**Formation Water (FW)**	**Salt (ppm)/Brine**	**Seawater (SW)**
$NaCl$	140316	$NaCl$	26400
$CaCo_3$	1628	$CaCl_2$	1180
$MgCl_2$	2856	KCl	400
$CaCl_2$	40287	$NaHCo_3$	7340
Na_2SO_4	2588	$MgCl_2.6H_2O$	5270
$NaHCO_3$	2016		

Table 5: Specification of media properties and flow parameters in the series of experiments at 40 ^{o}C and Corey exponents used for the history matching.

S/N	Media permeability (K)	Pore volume (cm^3)	Porosity (%)	Initial water saturation (S_{wi})	Injection rate (cm^3/s)	Corey exponents	
						N_w	N_o
1	7.01 ± 0.48	59.75 ± 0.74	30.43 ± 1.24	0.23	0.0167	3.83	6.00
2	5.03 ± 0.38	61.26 ± 1.23	31.20 ± 2.01	0.25	0.0125	6.88	3.56
3	6.01 ± 0.75	58.09 ± 0.87	29.58 ± 1.50	0.17	0.0083	2.64	12.78
4	6.50 ± 0.43	60.02 ± 1.57	30.57 ± 2.61	0.17	0.0167	3.81	2.98
5	5.02 ± 0.38	60.88 ± 0.69	31.01 ± 1.14	0.24	0.0125	7.02	7.99
6	4.59 ± 0.50	59.75 ± 0.38	30.43 ± 0.64	0.19	0.0083	5.77	3.94

Table 6: Specification of media properties and flow parameters in the series of experiments at 60 and 80 ^{o}C and LET parameters used for the history matching.

S/N	Media permeability (K)	Pore volume (cm^3)	Porosity (%)	Initial water saturation (S_{wi})	Injection rate (cm^3/s)	LET parameters					
						L_w	E_w	T_w	L_o	E_o	T_o
7	6.95 ± 0.47	59.75 ± 0.55	30.43 ± 0.92	0.28	0.0167	1.52	2.28	0.8	4.26	6.29	0.82
8	5.23 ± 0.41	61.26 ± 0.74	31.20 ± 1.21	0.25	0.0125	5.38	0.55	0.8	3.8	4.37	0.78
9	7.12 ± 0.98	58.09 ± 0.57	29.58 ± 0.99	0.26	0.0083	1.96	2.63	0.8	5.43	7.91	0.87
10	4.86 ± 0.27	60.88 ± 0.92	31.01 ± 1.51	0.11	0.0167	1.89	2.39	0.8	4.26	7.74	0.87
11	5.25 ± 0.41	61.56 ± 0.93	31.35 ± 1.51	0.25	0.0125	1.89	2.39	0.8	4.26	7.74	0.87
12	5.17 ± 0.60	61.87 ± 0.54	31.51 ± 0.88	0.24	0.0083	3.05	1.15	0.8	4.77	13.85	0.58
13	5.32 ± 0.31	61.64 ± 1.08	31.39 ± 1.75	0.12	0.0167	5.00	3.99	0.8	5.00	1.49	0.98
14	5.07 ± 0.39	62.39 ± 0.01	31.77 ± 0.02	0.26	0.0125	3.05	3.69	1.34	3.85	29.8	1.66
15	5.63 ± 0.68	60.50 ± 0.79	30.81 ± 1.31	0.21	0.0083	2.39	3.42	0.95	2.31	45.9	1.59
16	5.02 ± 0.29	60.50 ± 1.78	30.81 ± 2.95	0.11	0.0167	7.20	1.12	0.8	2.47	5.54	0.63
17	5.03 ± 0.38	60.50 ± 1.13	30.81 ± 1.87	0.24	0.0125	5.00	1.77	0.8	6.50	1.40	0.65
18	5.01 ± 0.57	60.50 ± 0.99	30.81 ± 1.64	0.21	0.0083	7.49	0.37	0.89	3.96	8.00	0.59

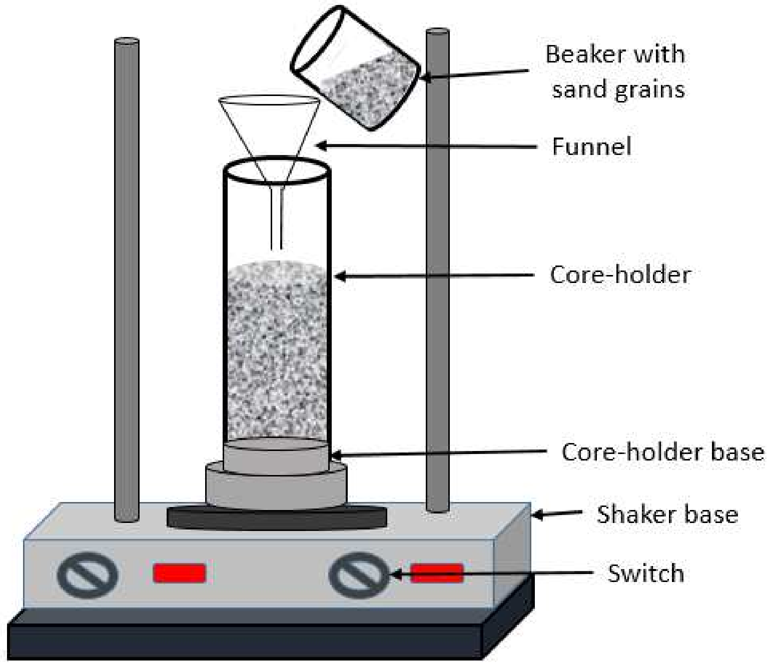

Figure 1: Schematic of the core-holder on the mechanical vibrator showing the sand packing process.

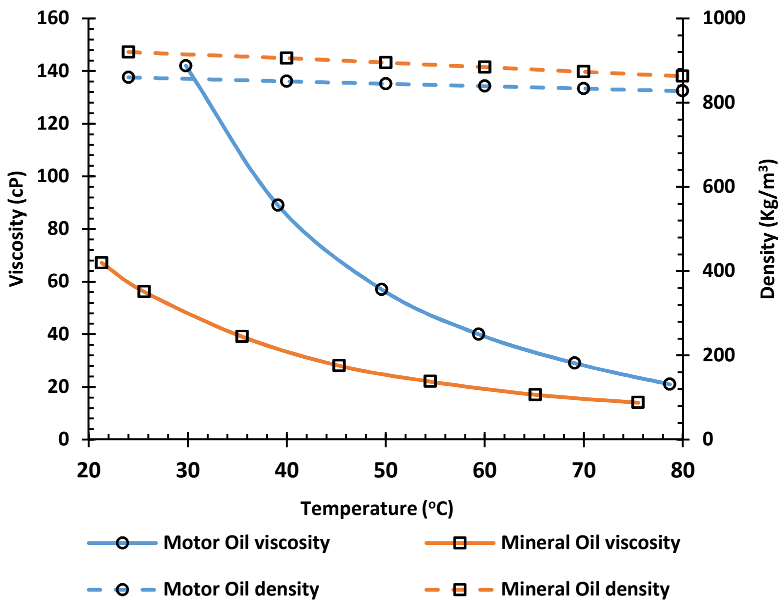

Figure 2: Plot of viscosity and density of oil sample against temperature at a shear rate of 510 s^{-1}.

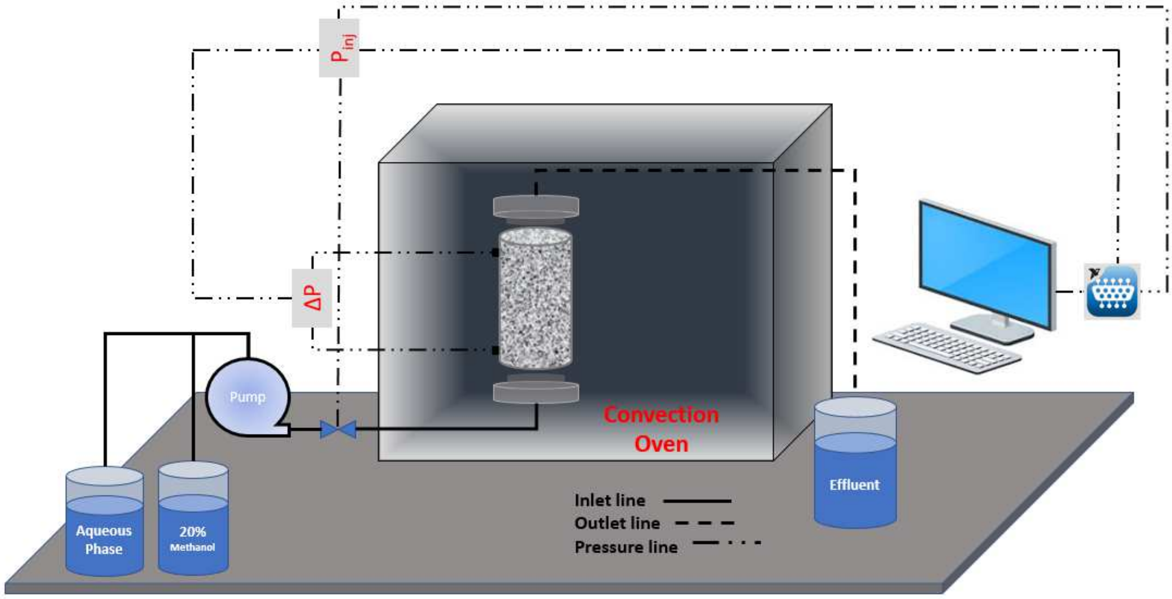

Figure 3: Schematic flow diagram of the experimental apparatus.

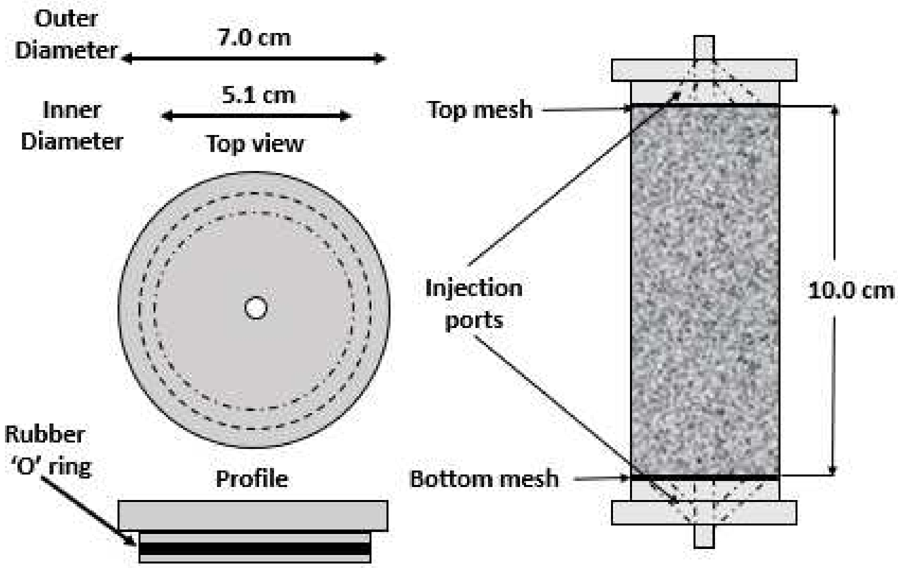

Figure 4: Diagrammatic representation of the aluminium core holder with its dimensions.

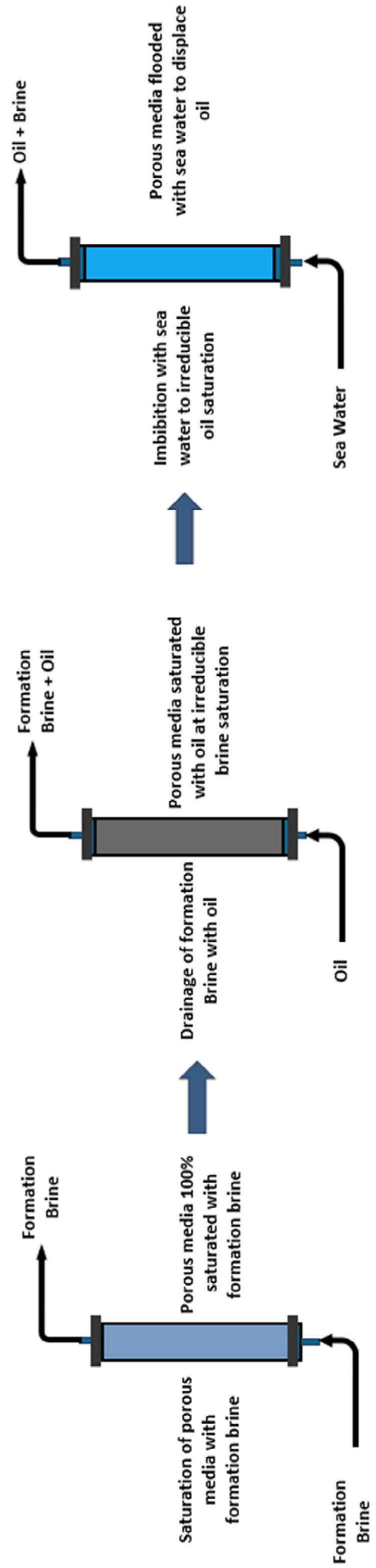

Figure 5: Schematic representation of the experimental flooding sequence.

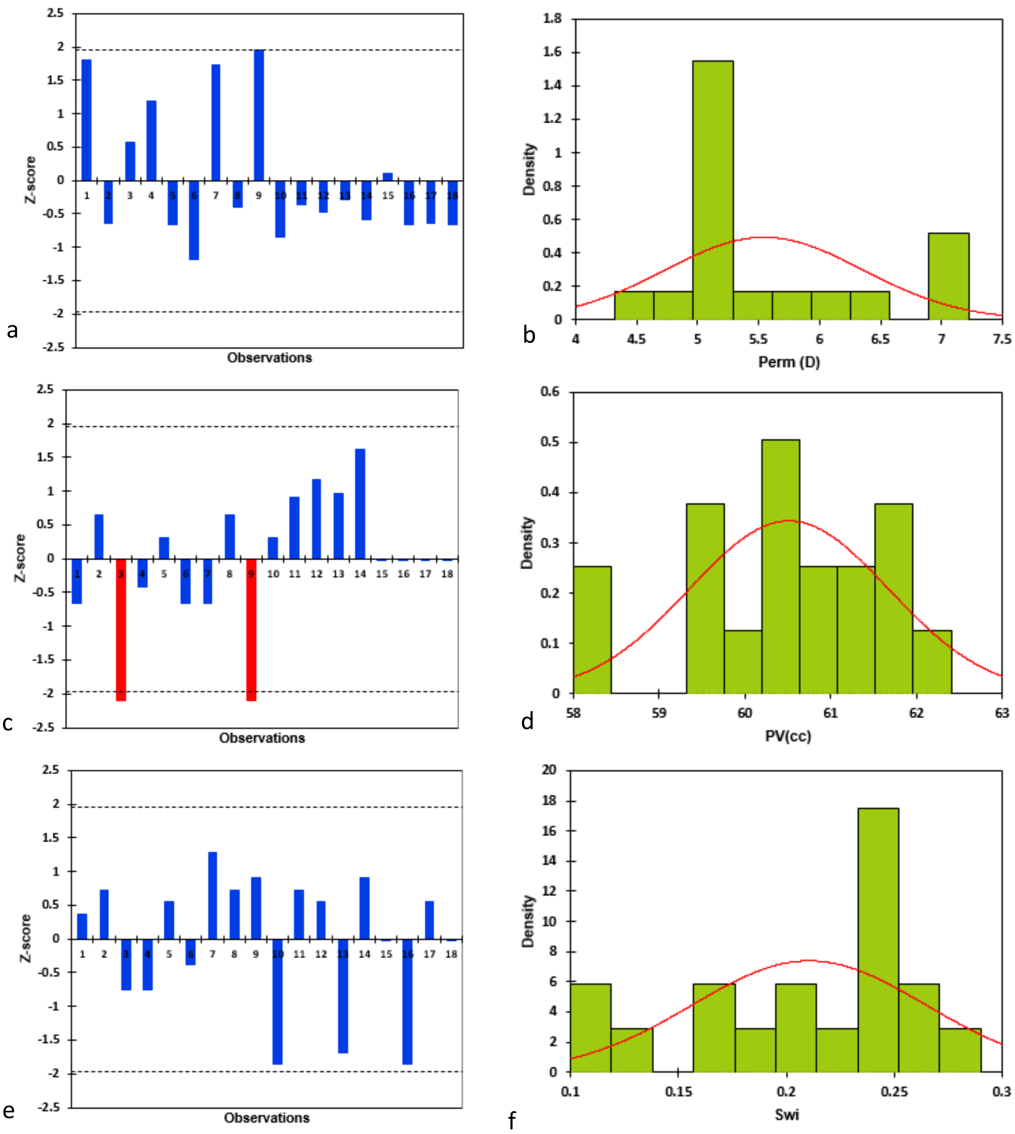

Figure 6: Z-score charts showing the outliers from Grubbs test (a. permeability, b. pore volume, c. initial water saturation) and histogram showing the normal distribution of the datasets (b. permeability, d. pore volume, f. initial water saturation).

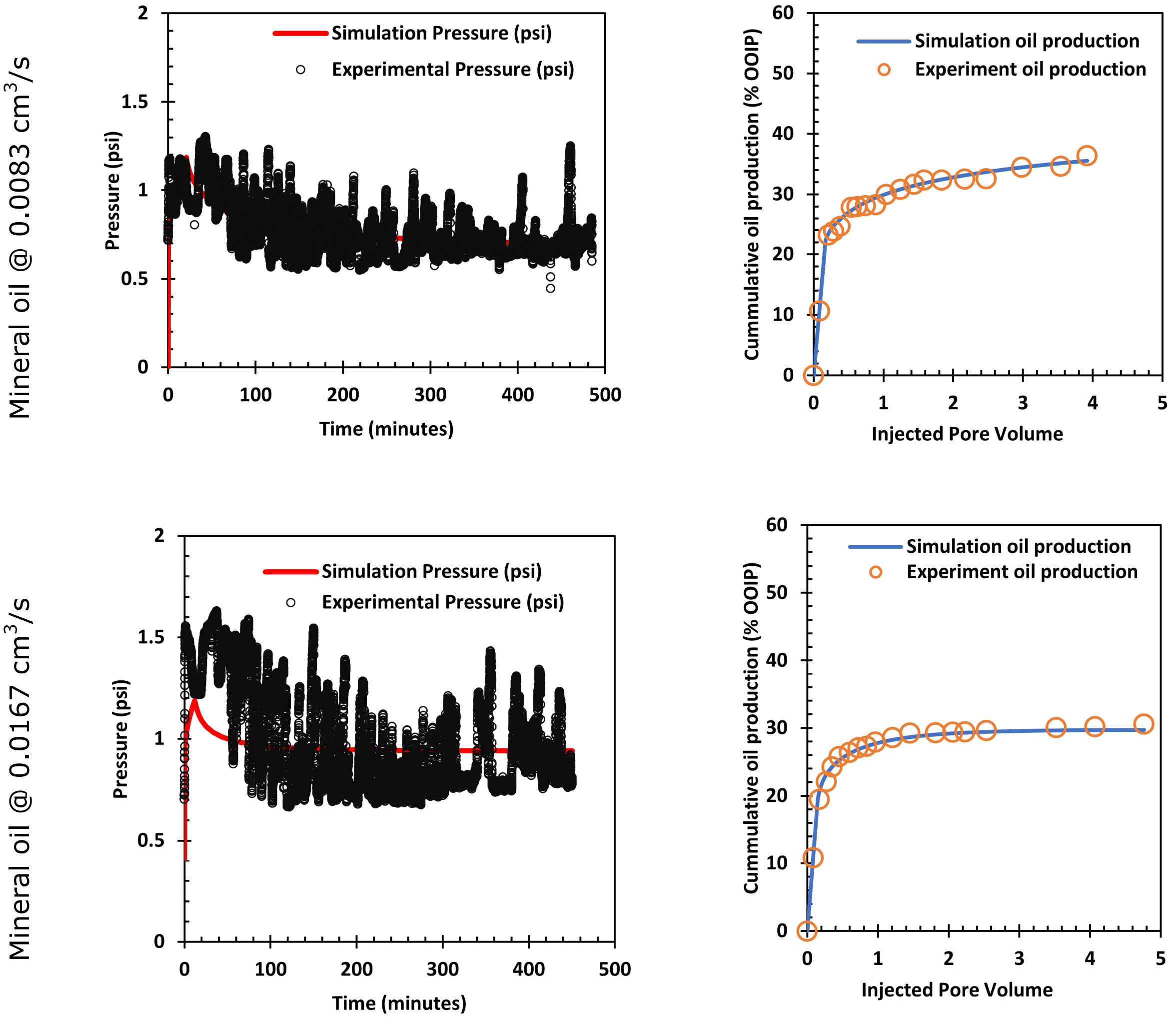

Figure 7: Experimental pressure data compared with history matched pressure from simulations (column 1). Experimental cumulative oil produced as a percentage of the OOIP against number of injected pore volume of water, compared with the production from history matched simulations corresponding to the pressure curve conditions under same condition as the pressure profiles (column 2).

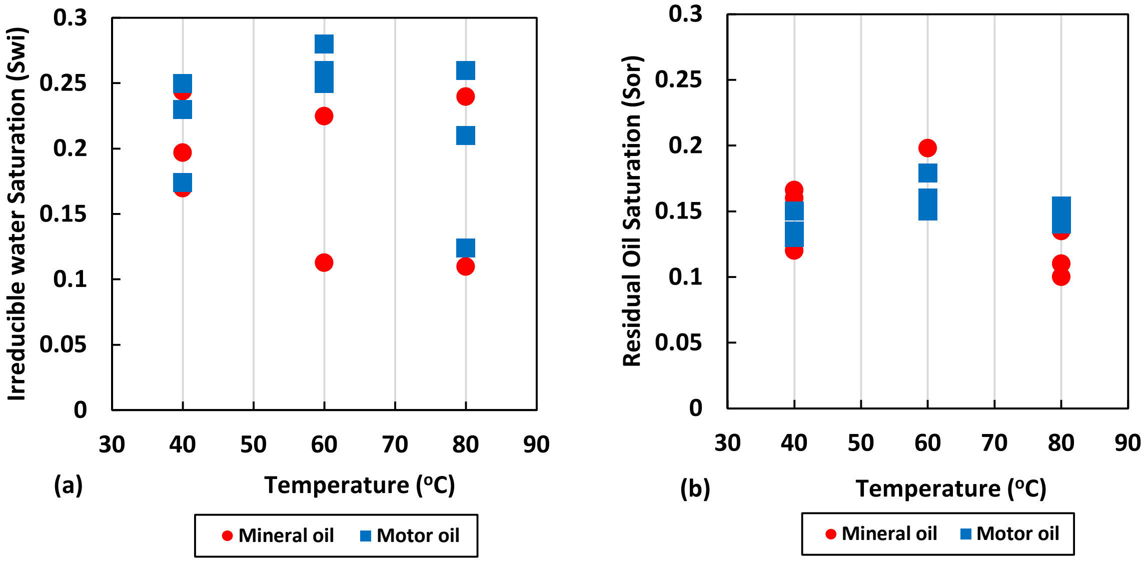

Figure 8: Plot of irreducible; (a) water saturation and (b) residual oil saturation for all the experiments conducted.

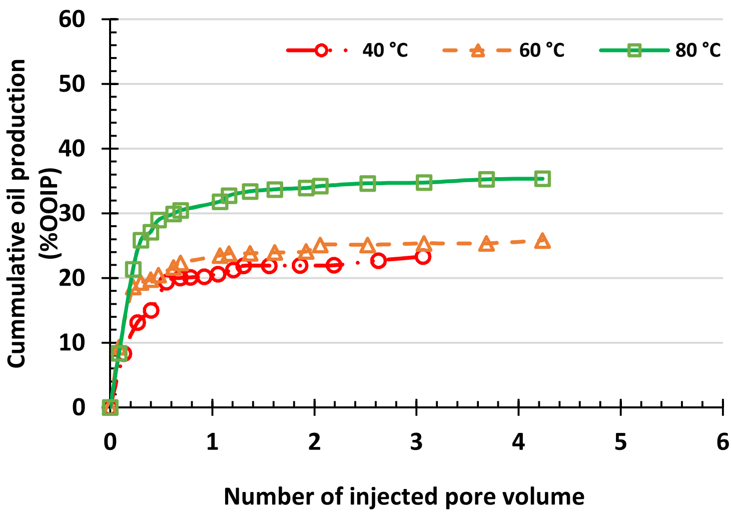

(a)

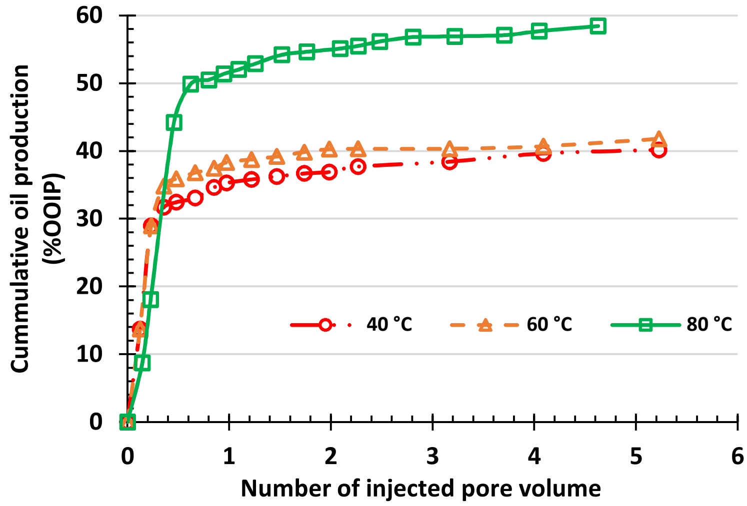

(b)

Figure 9: Cumulative oil production vs pore volumes injection for experimental runs on Motor oil at (a) 0.0083, and (b) 0.0125 cm^3/s under varying temperatures.

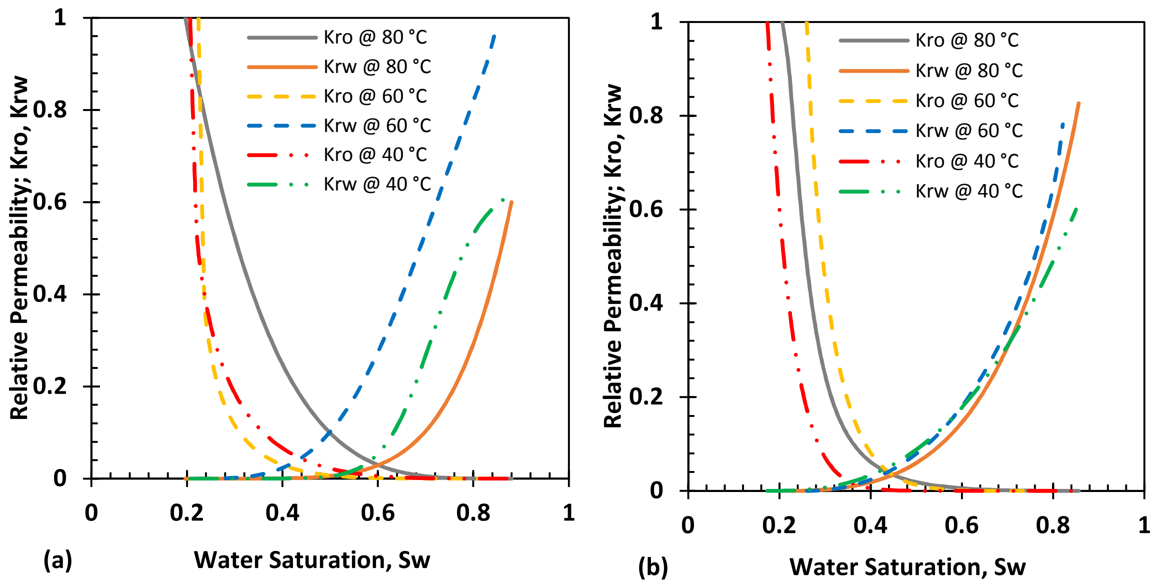

Figure 10: Relative permeability curves for the experiments done on sandpacks at 0.0083 cm^3/s for (a) mineral oil, and (b) motor oil.

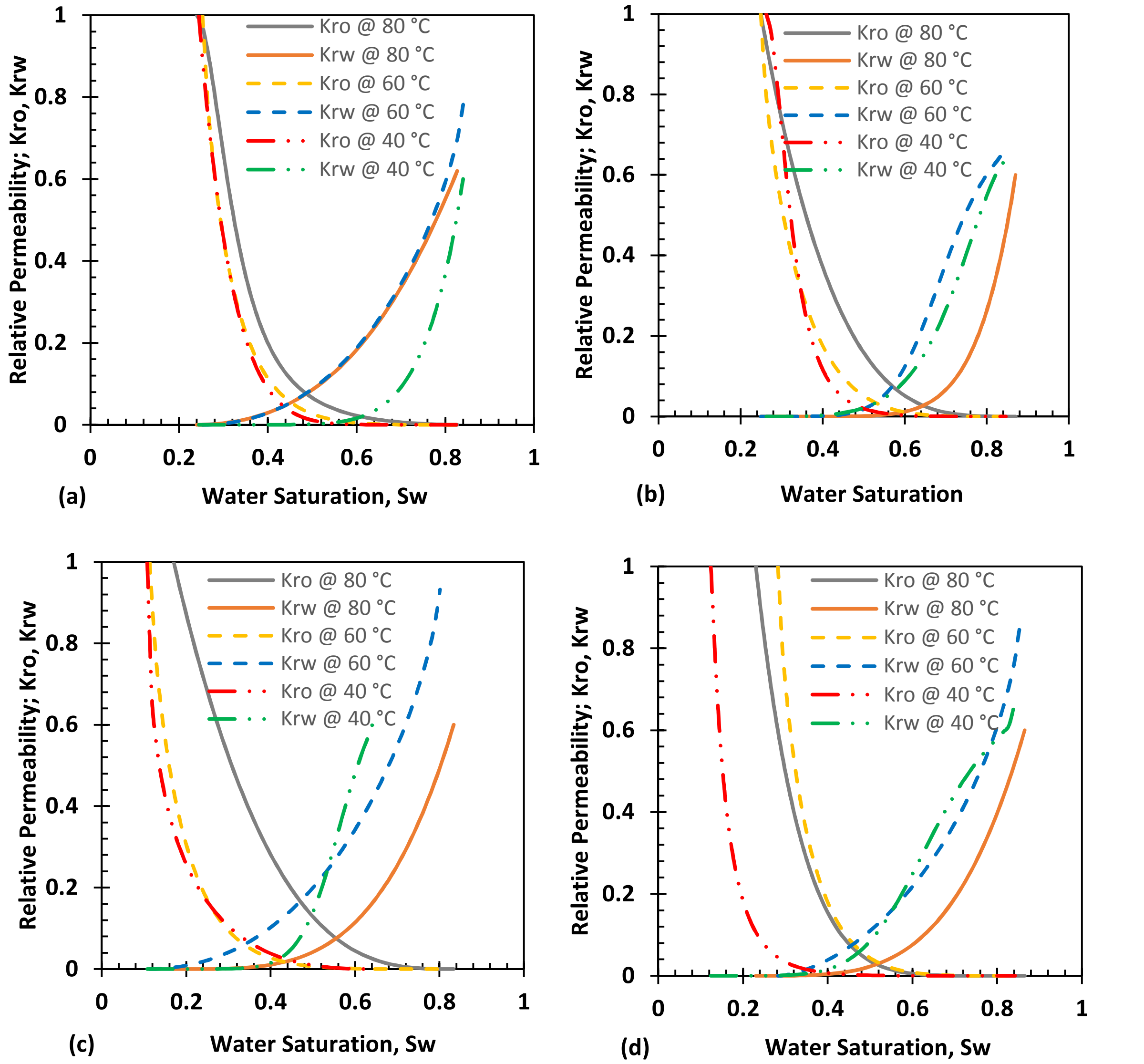

Figure 11: Relative permeability curves for the experiments done on sandpacks at (a) mineral oil – 0.0125 cm^3/s, (b) motor oil - 0.0125 cm^3/s, (c) mineral oil – 0.0167 cm^3/s, and (d) motor oil – 0.0167 cm^3/s.

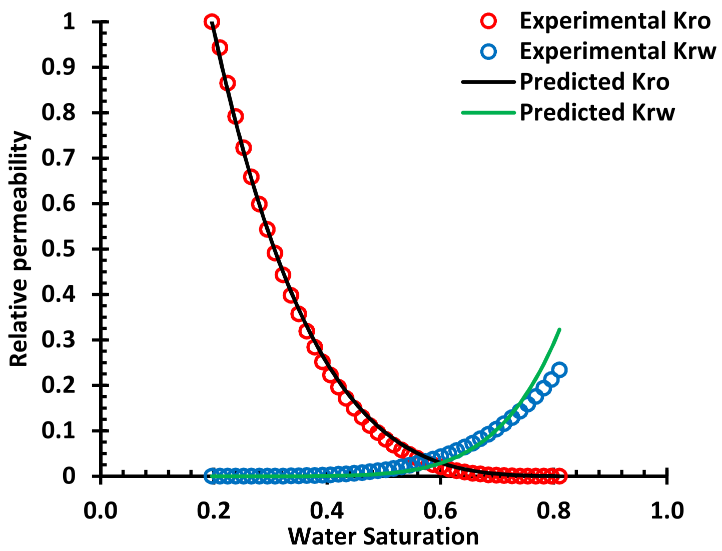

Figure 12:Comparison between the experimental relative permeability values and outputs predicted from the empirical model with the modified empirical constants.

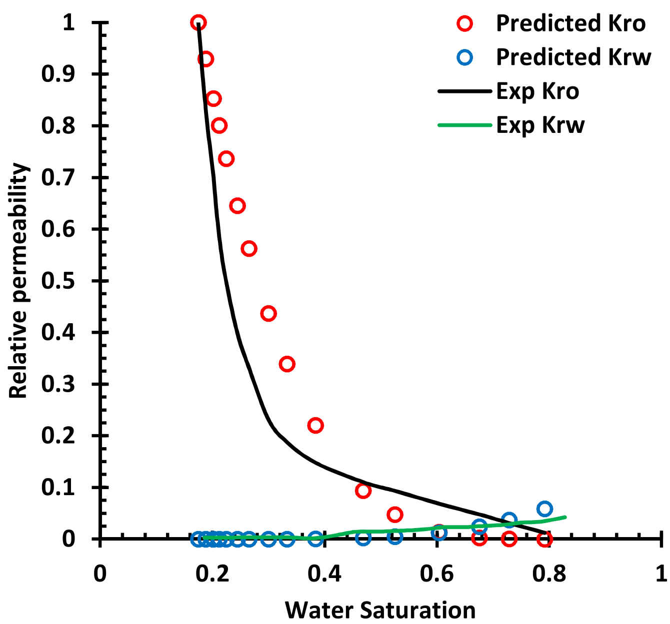

Figure 13: Comparison between experimental relative permeability from Ashrafi et al., (2012) and outputs generated the modified empirical constants in this study.